

RESEARCH ARTICLE

IP6K1 is essential for chromatoid body formation and temporal regulation of *Tnp2* and *Prm2* expression in mouse spermatids

Aushaq Bashir Malla^{1,2} and Rashna Bhandari^{1,*}

ABSTRACT

Inositol hexakisphosphate kinases (IP6Ks) are enzymes that synthesise the inositol pyrophosphate 5-diphosphoinositol pentakisphosphate (5-IP₇), which is known to regulate several physiological processes. Deletion of IP6K1, but not other IP6K isoforms, causes sterility in male mice. Here, we present a detailed investigation of the specific function of IP6K1 in spermatogenesis. Within the mouse testis, IP6K1 is expressed at high levels in late stage pachytene spermatocytes and in round spermatids. We found IP6K1 to be a novel component of the chromatoid body, a cytoplasmic granule found in round spermatids that is composed of RNA and RNA-binding proteins, and noted that this structure is absent in *Ip6k1*^{-/-} round spermatids. Furthermore, juvenile spermatids from *Ip6k1*^{-/-} mice display premature expression of the transition protein TNP2 and the protamine PRM2 due to translational derepression. The aberrant localisation of these key sperm-specific chromatin components, together with the persistence of somatic histones, results in abnormal spermatid elongation, failure to complete spermatid differentiation and azoospermia in these mice. Our study thus identifies IP6K1 as an indispensable factor in the temporal regulation of male germ cell differentiation.

This article has an associated First Person interview with the first author of the paper.

KEY WORDS: Spermatogenesis, Spermiogenesis, Chromatoid body, Protamine, Transition protein, Inositol hexakisphosphate kinase

INTRODUCTION

Inositol hexakisphosphate kinases (IP6Ks) are evolutionarily conserved inositol phosphate kinases that generate the small molecule messenger, 5-diphosphoinositol pentakisphosphate (5PP-IP₅ or 5-IP₇) from inositol hexakisphosphate (IP₆) (Saiardi et al., 1999; Thomas and Potter, 2014). There are three mammalian IP6K isoforms, IP6K1, IP6K2 and IP6K3, which have a highly conserved C-terminus and a more diverse N-terminus (Wang et al., 2014). IP6K1 and IP6K2 are expressed ubiquitously with varying levels of expression in different tissues (Saiardi et al., 1999), whereas IP6K3 is highly expressed in the cerebellum and skeletal muscle (Saiardi et al., 2001; Fu et al., 2015; Moritoh et al., 2016). Genomic deletion of *Ip6k1* in mice leads to a dramatic loss of male

fertility (Bhandari et al., 2008), but *Ip6k2*- and *Ip6k3*-knockout mice breed normally (Morrison et al., 2009; Fu et al., 2015; Moritoh et al., 2016). The specific occurrence of male sterility in *Ip6k1*-knockout mice, but not in mice devoid of the other IP6K isoforms, suggests a distinct role for IP6K1 in spermatogenesis.

Spermatogenesis is a complex and dynamic process during which germ cells develop in the seminiferous tubules of the testis, with Sertoli cells providing them with structural and metabolic support. The process of spermatogenesis involves three phases – mitotic, meiotic and haploid. During the mitotic phase, spermatogonial stem cells self-renew and produce spermatogonia that proliferate and differentiate, eventually generating primary spermatocytes. Primary spermatocytes undergo two successive meiotic divisions to produce haploid round spermatids. Round spermatids undergo a lengthy phase of spermatid differentiation called spermiogenesis. During this process, round spermatids go through complex biochemical and morphological changes resulting in formation of the acrosome and sperm tail, removal of excess cytoplasm and extensive nuclear condensation (Russell et al., 1990). Mature spermatids are released from the testis and are stored in the epididymis prior to ejaculation.

In mice, the cycle of the seminiferous epithelium is divided into 12 stages (stages I–XII). Each stage represents a particular arrangement of different types of developmentally synchronised germ cells as seen in a cross-section of a seminiferous tubule (Russell et al., 1990; Ahmed and de Rooij, 2009). Spermiogenesis is subdivided into 16 steps (steps 1–16) based on changes in acrosome structure and nuclear compaction of maturing spermatids (Russell et al., 1990; Ahmed and de Rooij, 2009). Spermiogenesis is accompanied by extensive chromatin reorganisation during which most of the nucleosomal histones are initially replaced by transition proteins (TNP1 and TNP2) and subsequently by protamines (PRM1 and PRM2) (Rousseaux et al., 2008). Differentiation of round spermatids into compact elongated spermatids makes the latter transcriptionally inactive, leading to global gene silencing due to extensive chromatin condensation (Braun, 1998). Genes that are required during the final steps of spermiogenesis are transcribed in round spermatids and their mRNAs are stored in a translationally repressed state until their timely translation is initiated (Braun, 1998). Premature expression of TNP2, PRM1 or PRM2 has been associated with defective spermatid morphology and infertility in mice (Lee et al., 1995; Tseden et al., 2007; Fukuda et al., 2013).

While previous histologic examination of *Ip6k1*^{-/-} mice revealed few advanced spermatids in the testes and no sperm in the epididymis, the functional basis for spermiogenesis failure in these mice was not explored (Bhandari et al., 2008). In this study, we show that IP6K1 is highly expressed in round spermatids. Loss of IP6K1 leads to failure in spermatid differentiation due to defects in elongation and condensation of sperm nuclei. We found that in round spermatids, IP6K1 is enriched in a perinuclear ribonucleoprotein complex called the chromatoid body, and noted that the chromatoid body is absent or fragmented in *Ip6k1*^{-/-}

¹Laboratory of Cell Signalling, Centre for DNA Fingerprinting and Diagnostics, Hyderabad, Telangana 500001, India. ²Graduate Studies, Manipal University, Manipal, Karnataka 576104, India.

*Author for correspondence (rashna@cdf.org.in)

 R.B., 0000-0003-3101-0204

spermatids. We also observed premature synthesis of TNP2 and PRM2 in round spermatids from juvenile *Ip6k1*^{-/-} mice, suggesting that IP6K1 is an important component of the post-transcriptional regulatory machinery of testicular germ cells, and therefore an indispensable regulator of male germ cell differentiation.

RESULTS

Loss of IP6K1 in mice results in azoospermia

When *Ip6k1*^{-/-} female mice were mated with *Ip6k1*^{-/-} male mice, no pregnancies were observed, but when the same females were mated with heterozygous male mice, pups were born according to Mendelian ratios (Bhandari et al., 2008), indicating that IP6K1 is necessary for gametogenesis in males but not in females. On pairing adult *Ip6k1*^{-/-} males with wild-type females, we found that these mice could successfully mount the females and produce coital plugs, suggesting that defects in their male sexual behaviour are not responsible for their infertility. We dissected and compared the testes and epididymides of adult (2–3 months old) *Ip6k1*^{+/+} and *Ip6k1*^{-/-} male mice. Testes and epididymides are smaller in *Ip6k1*^{-/-} mice compared to those in their *Ip6k1*^{+/+} littermates, but do not show any gross morphological defects (Fig. 1A). To determine whether the reduction in epididymis and testis size can be attributed to the lower body weight of *Ip6k1*^{-/-} mice (Bhandari et al., 2008), we normalised the average epididymis or testis weight of each mouse to its body weight, and noted that this ratio was reduced by ~30% for both tissues in *Ip6k1*^{-/-} compared to that in *Ip6k1*^{+/+} mice (Fig. 1B,C). A reduction in serum testosterone levels has been shown to correlate with reduced weight of the testis and epididymis (Xu et al., 2007; Luria et al., 2009), but we observed no significant difference between serum testosterone levels in *Ip6k1*^{+/+} and *Ip6k1*^{-/-} mice (Fig. 1D). Histological examination of epididymides revealed densely packed mature spermatozoa in *Ip6k1*^{+/+} mice, but abnormal round cells in the epididymidal lumen of *Ip6k1*^{-/-} mice (Fig. 1E). Germ cells isolated from the epididymal lumen were examined more closely through DAPI staining to reveal mature spermatozoa in *Ip6k1*^{+/+} mice, and primarily round cells with a few abnormal elongated spermatozoa in *Ip6k1*^{-/-} mice (Fig. 1F). This was reflected as a dramatic decrease in the sperm count in *Ip6k1*^{-/-} mice (Fig. 1G). TUNEL staining of epididymal sections from *Ip6k1*^{-/-} mice revealed that nearly all the germ cells in the epididymal lumen carry fragmented DNA, suggesting that they are undergoing degeneration (Fig. 1H). These results clearly demonstrate that male infertility associated with the loss of IP6K1 is primarily due to azoospermia, that is, the absence of mature spermatozoa in the epididymis.

IP6K1 is expressed at high levels in round spermatids

Ip6k1 is known to be actively transcribed in a variety of mouse tissues but its transcript levels are specifically enriched in testis and brain (Saiardi et al., 1999). To gain further insight into the role of IP6K1 in male fertility, we examined its expression profile during the course of sperm development in mouse testes. Testes collected from 14-, 18-, 28-, 35- and 60-day-old mice were subjected to immunoblotting to detect IP6K1 levels (Fig. 2A). 14 day postpartum (dpp) testes contain Sertoli cells, spermatogonia, leptotene, zygotene and early pachytene spermatocytes; 18 dpp testes possess spermatogonia, early and late pachytene spermatocytes; 28 ddp testes contain round spermatids and early elongating spermatids in addition to these germ cells, and 35 dpp and adult (60 dpp) testes contain all germ cells including elongated spermatids (Bellvé et al., 1977; Kluin et al., 1982). IP6K1 was detected at low levels in 14 dpp testes; its expression increased

significantly in 18 dpp testes and continued to rise during later stages of sperm development, suggesting that this protein is more abundant in late meiotic and post-meiotic germ cells (Fig. 2A,B).

To identify the precise cell types expressing *Ip6k1*, we performed immunofluorescence to detect IP6K1 in testis sections from *Ip6k1*^{+/+} mice, with a *Ip6k1*^{-/-} section serving as the negative control (Fig. 2C,D). IP6K1 was localised to the cytoplasm of late pachytene (Fig. 2Ci) and diplotene spermatocytes (Fig. 2Cii). In post-meiotic round spermatids, IP6K1 was expressed at high levels in the cytoplasm and appeared concentrated in cytoplasmic granules (Fig. 2Ciii). We did not detect intense IP6K1 staining in Sertoli cells, spermatogonia, leptotene, zygotene, or early pachytene spermatocytes (Fig. 2C). However, as 14 dpp tubules contain only these cell types (Bellvé et al., 1977), it is likely that some of these express low levels of IP6K1. This possibility is supported by the observation that the regions of the *Ip6k1*^{+/+} sections containing these cells (Fig. 2C) show a higher immunofluorescence signal than the background observed in *Ip6k1*^{-/-} sections (Fig. 2D). The increase in IP6K1 levels in 60 dpp testes (Fig. 2A,B) may be due to its higher expression in round spermatids which constitute the major population of testicular cells in adult testis. The high expression level of IP6K1 in late spermatocytes and round spermatids (Fig. 2E) is commensurate with a role for this protein in spermiogenesis.

Ip6k1 deletion leads to abnormalities in spermatid elongation and condensation

Histological examination of stage X/XI, and stage I tubules from 2-month-old *Ip6k1*^{+/+} and *Ip6k1*^{-/-} mice revealed no obvious differences in the composition and arrangement of cells (Fig. S1A). Although elongating spermatids are present in the earlier developmental stages, stage VIII tubules, which normally contain mature spermatids close to the lumen, showed no condensed spermatids in *Ip6k1*^{-/-} testes (Fig. S1A), suggesting that elongating spermatids are lost during development in these mice. Germ cell layers towards the basement membrane of seminiferous tubule cross-sections were largely unaltered between *Ip6k1*^{+/+} and *Ip6k1*^{-/-} mice, with no detectable changes in spermatogonia and spermatocytes (Figs S1A and S2). This observation was corroborated by flow cytometry analysis of DNA content in isolated testicular cells. *Ip6k1*^{+/+} testicular cells revealed four different peaks corresponding to fully condensed elongated spermatids (HC), round spermatids (1C), spermatogonia and somatic cells (2C), and primary spermatocytes (4C) (Krishnamurthy et al., 2000) (Fig. S1B). In *Ip6k1*^{-/-} testicular cells, the percentage of elongated spermatids (HC) was drastically reduced (Fig. S1B,C) and there was a proportional increase in the 4C and 2C cell populations. Interestingly, the *Ip6k1*^{-/-} HC peak could not be clearly resolved from 1C, which is suggestive of reduced DNA compaction in these spermatids (Fig. S1B).

To closely examine the development of *Ip6k1*^{-/-} spermatids, we identified the 16 developmental steps of spermiogenesis based on the shape of the nucleus and acrosome (Russell et al., 1990), by co-staining testis sections with DAPI and peanut agglutinin (PNA), a lectin that binds to glycoconjugates on the outer acrosomal membrane (Aviles et al., 1997) (Fig. S2). Step 1 to 12 spermatids are observed in stages I through XII, and step 13 to 16 spermatids are seen in stages I through VIII of the seminiferous epithelium (Fig. 2E). Analysis of adult stage XI seminiferous tubules revealed that, in *Ip6k1*^{-/-} mice, the round spermatids advance to step 10–11 elongating spermatids, but their nuclear morphology is abnormal (Fig. 3A). By stage XII (step 12) *Ip6k1*^{+/+} spermatids attain their condensed comma shape, whereas *Ip6k1*^{-/-} tubules show

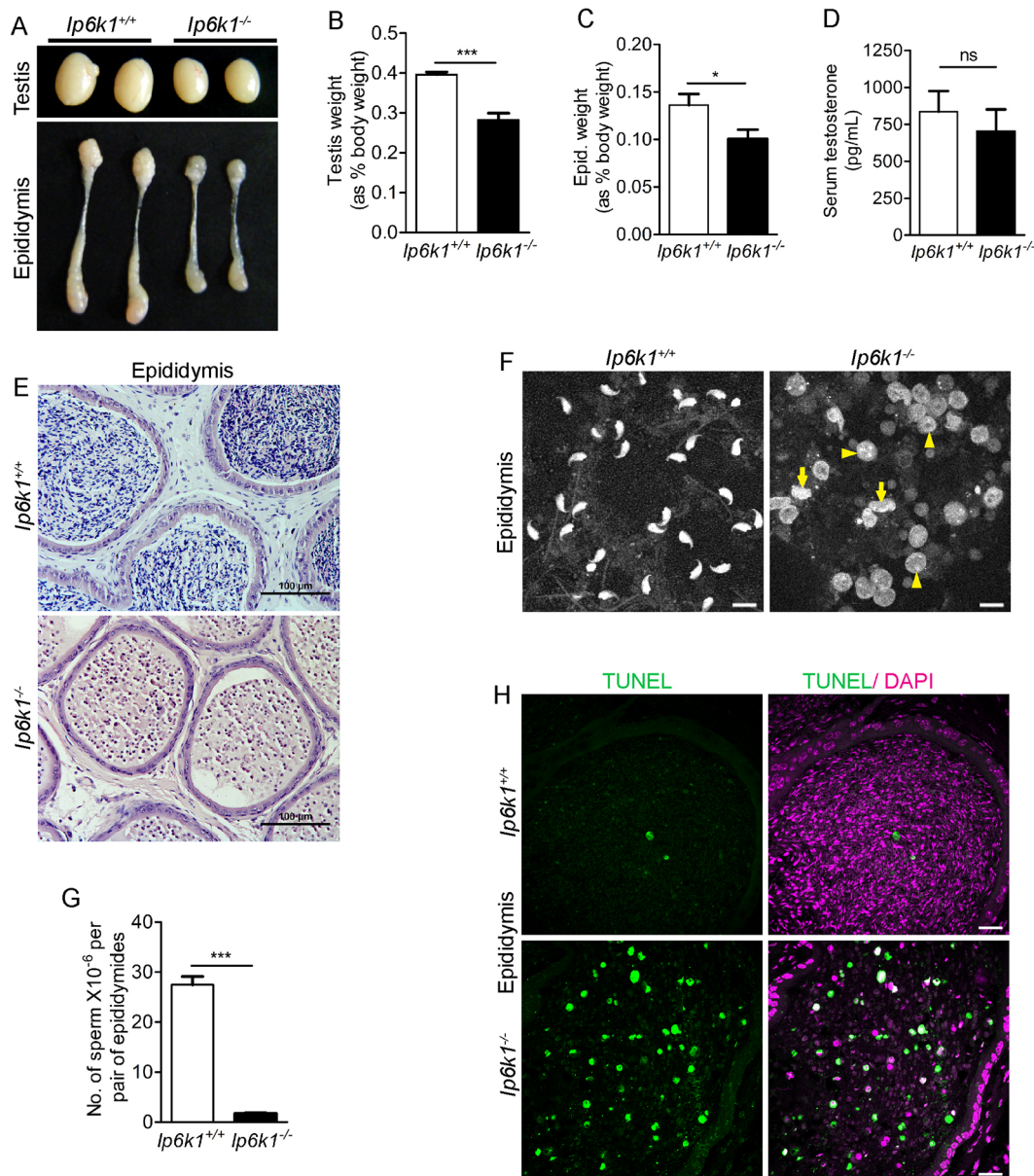


Fig. 1. Male *Ip6k1*^{-/-} mice are azoospermic. (A) Images of testes and epididymides isolated from *Ip6k1*^{+/+} and *Ip6k1*^{-/-} mice. The sizes of both organs are reduced in *Ip6k1*^{-/-} compared to in *Ip6k1*^{+/+} mice. (B) Comparison of testis weight between *Ip6k1*^{+/+} and *Ip6k1*^{-/-} mice. When normalised to body weight, testis weight is reduced by ~30% in *Ip6k1*^{-/-} compared to in *Ip6k1*^{+/+} mice. *n*=7 mice of each genotype. (C) Comparison of epididymal weight between *Ip6k1*^{+/+} and *Ip6k1*^{-/-} mice. When normalised to body weight, epididymal weights are reduced by ~30% in *Ip6k1*^{-/-} compared to *Ip6k1*^{+/+} mice. *n*=8 mice of each genotype. (D) Serum concentration of testosterone (pg/ml) in *Ip6k1*^{+/+} and *Ip6k1*^{-/-} male mice. *n*=4 for *Ip6k1*^{+/+} and *n*=5 for *Ip6k1*^{-/-} mice. (E) Haematoxylin and eosin-stained epididymal cross-sections of adult *Ip6k1*^{+/+} and *Ip6k1*^{-/-} mice. *Ip6k1*^{+/+} epididymides are fully occupied by mature spermatozoa but *Ip6k1*^{-/-} epididymides only contain degenerating round cells. Scale bars: 100 μ m. (F) DAPI-stained epididymal germ cells isolated from epididymides of *Ip6k1*^{+/+} and *Ip6k1*^{-/-} mice. *Ip6k1*^{+/+} epididymides are occupied by mature spermatozoa but *Ip6k1*^{-/-} epididymides only contain abnormally condensed spermatids (arrows) and round nuclei (arrowheads). Scale bars: 10 μ m. (G) Epididymal sperm count from *Ip6k1*^{+/+} and *Ip6k1*^{-/-} adult mice. No fully mature comma-shaped spermatozoa were observed in *Ip6k1*^{-/-} mice but the abnormally elongated spermatids (arrows in F) were counted. The epididymal sperm count was drastically reduced in *Ip6k1*^{-/-} mice. *n*=5 mice of each genotype. (H) TUNEL staining (green) in *Ip6k1*^{+/+} and *Ip6k1*^{-/-} epididymides. Intense TUNEL staining of the round cells present in *Ip6k1*^{-/-} epididymides confirmed that these are dead cells. Nuclei were counterstained with DAPI (magenta). White spots (overlap of magenta and green) indicate TUNEL-positive nuclei. Scale bars: 20 μ m. All quantitative data are mean \pm s.e.m. **P*≤0.05; ****P*≤0.0001; ns, *P*=0.54, not significant (two-tailed unpaired Student's *t*-test).

irregularly shaped decondensed spermatid nuclei similar to those seen in stage XI (Fig. 3B). By step 14 (stage II–III), *Ip6k1*^{+/+} spermatid nuclei were further condensed but *Ip6k1*^{-/-} spermatids remained decondensed (Fig. 3C). Finally, as observed in the histological sections (Fig. S1A), stage VIII (step 16) fully condensed ready-to-release spermatids were seen in *Ip6k1*^{+/+} tubules, but were entirely absent in *Ip6k1*^{-/-} mice (Fig. 3D).

Stage VIII tubules also show step 8 round spermatids with a fully developed acrosome, which appear identical in *Ip6k1*^{+/+} and *Ip6k1*^{-/-} mice. This was observed more clearly in isolated round spermatids stained with PNA (Fig. S3A).

For a closer examination of spermatid morphology, we isolated elongated spermatids corresponding to steps 13 to 16 of spermatid differentiation by undertaking transillumination-assisted

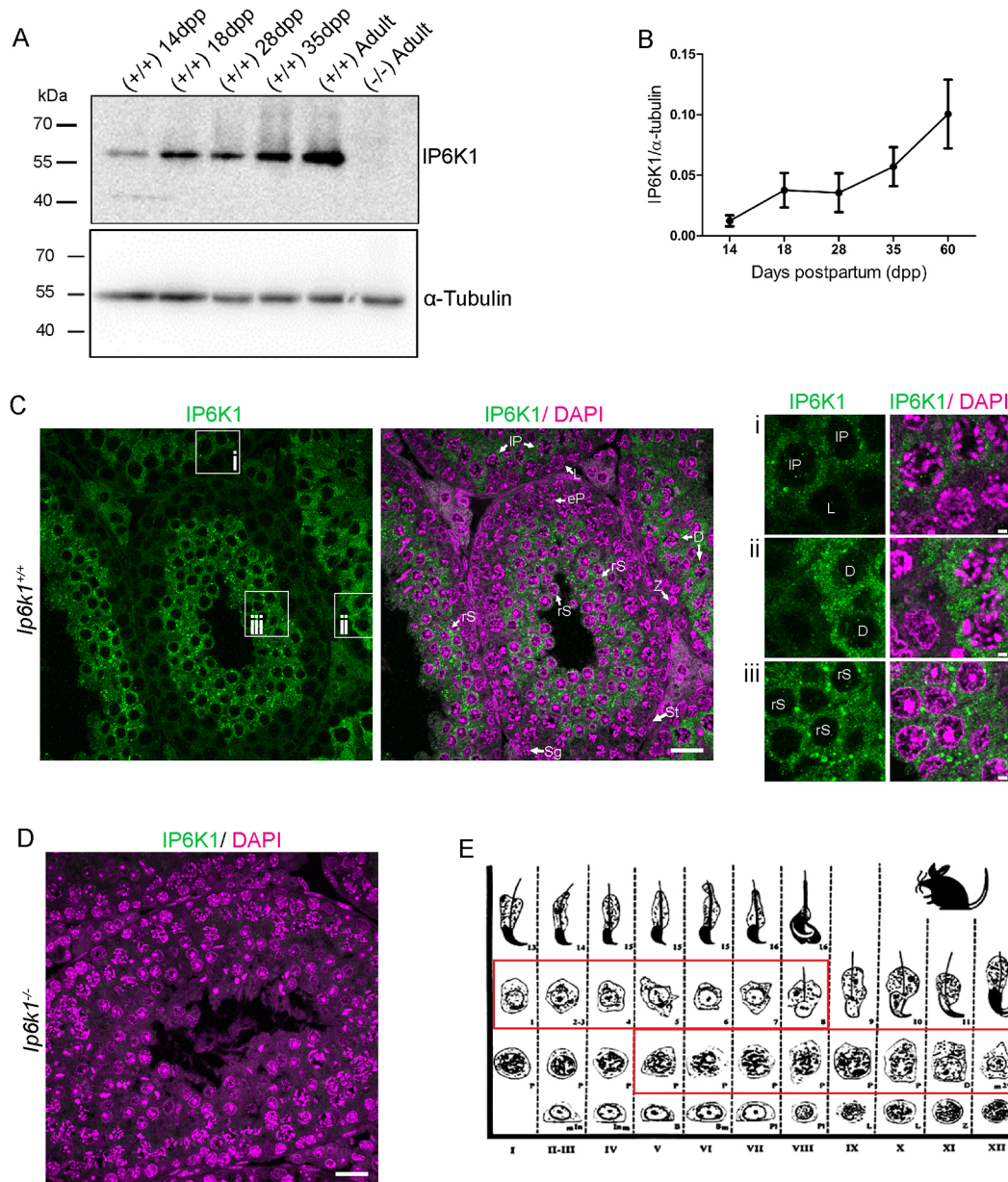


Fig. 2. IP6K1 is expressed in meiotic and post-meiotic germ cells in mouse testes. (A) Western blot analysis of IP6K1 in 14 dpp, 18 dpp, 28 dpp, 35 dpp and adult (60 dpp) testes of *Ip6k1*^{+/+} mice (+/+) and in adult testes of *Ip6k1*^{-/-} mice (-/-). α -tubulin was used as a loading control. (B) Quantification of IP6K1 expression in juvenile and adult testes of *Ip6k1*^{+/+} mice. Values indicate mean \pm s.e.m.; $n=3$ for each age group. IP6K1 expression was detected at low levels in 14 dpp testes and increased with the progression of spermatogenesis. (C) Immunostaining of 35 dpp *Ip6k1*^{+/+} testis for the detection of IP6K1 (green). Nuclei are stained with DAPI (magenta). Boxed areas in C were magnified and are shown as insets i, ii and iii. Ci shows IP6K1 expression in late pachytene spermatocytes (labelled IP). Cii shows IP6K1 expression in diplotene spermatocytes (labelled D). Ciii reveals a high level of IP6K1 expression in round spermatids (labelled rS). The other cell types marked are Sertoli cells (St), spermatogonia (Sg), leptotene (L), zygotene (Z) and early pachytene spermatocytes (eP). Inset Ci is from a stage X tubule, Cii is from a stage XI tubule, and Ciii represents stages II–VI. Scale bars: 20 μ m (insets 2 μ m). (D) Immunostaining of 35 dpp *Ip6k1*^{-/-} testis for the detection of IP6K1 (green) as a negative control. Nuclei are stained with DAPI (magenta). Scale bar: 20 μ m. (E) Stage-wise expression of IP6K1 in mouse testis shown in a scheme modified from Russell et al., 1990. Mouse spermatogenic cell staging map reprinted with permission from Cache River Press, St Louis, MO, USA. Cells showing high levels of cytoplasmic IP6K1 expression are boxed in red.

microdissection of seminiferous tubules, and stained them with DAPI to detect their nuclei. *Ip6k1*^{-/-} spermatids displayed irregularly shaped heads and a bent or blunt apex, lacking the typical hook-shaped appearance of *Ip6k1*^{+/+} spermatids (Fig. 3E). Consistent with this, transmission electron microscopy of elongating/elongated spermatids revealed less condensed and loosely packed deformed nuclei with uneven density in *Ip6k1*^{-/-} spermatids (Fig. 3F,G) in comparison to tightly packed and homogeneously condensed *Ip6k1*^{+/+} spermatids (Fig. 3H,I). Misshapen sperm heads have also been shown to arise due

to anomalies in the formation of the manchette, a transient tubulin-rich structure formed around the nucleus in step 10–12 elongating spermatids (Kierszenbaum et al., 2007). We stained testis sections to detect α -tubulin, which marks the manchette, and noted normal formation of this structure despite the abnormal shape of *Ip6k1*^{-/-} spermatid nuclei (Fig. S3B). Taken together, these data suggest that improper nuclear condensation of *Ip6k1*^{-/-} elongating spermatids is not due to defects in acrosome or manchette formation, and may arise due to deficiencies in sperm DNA condensation.

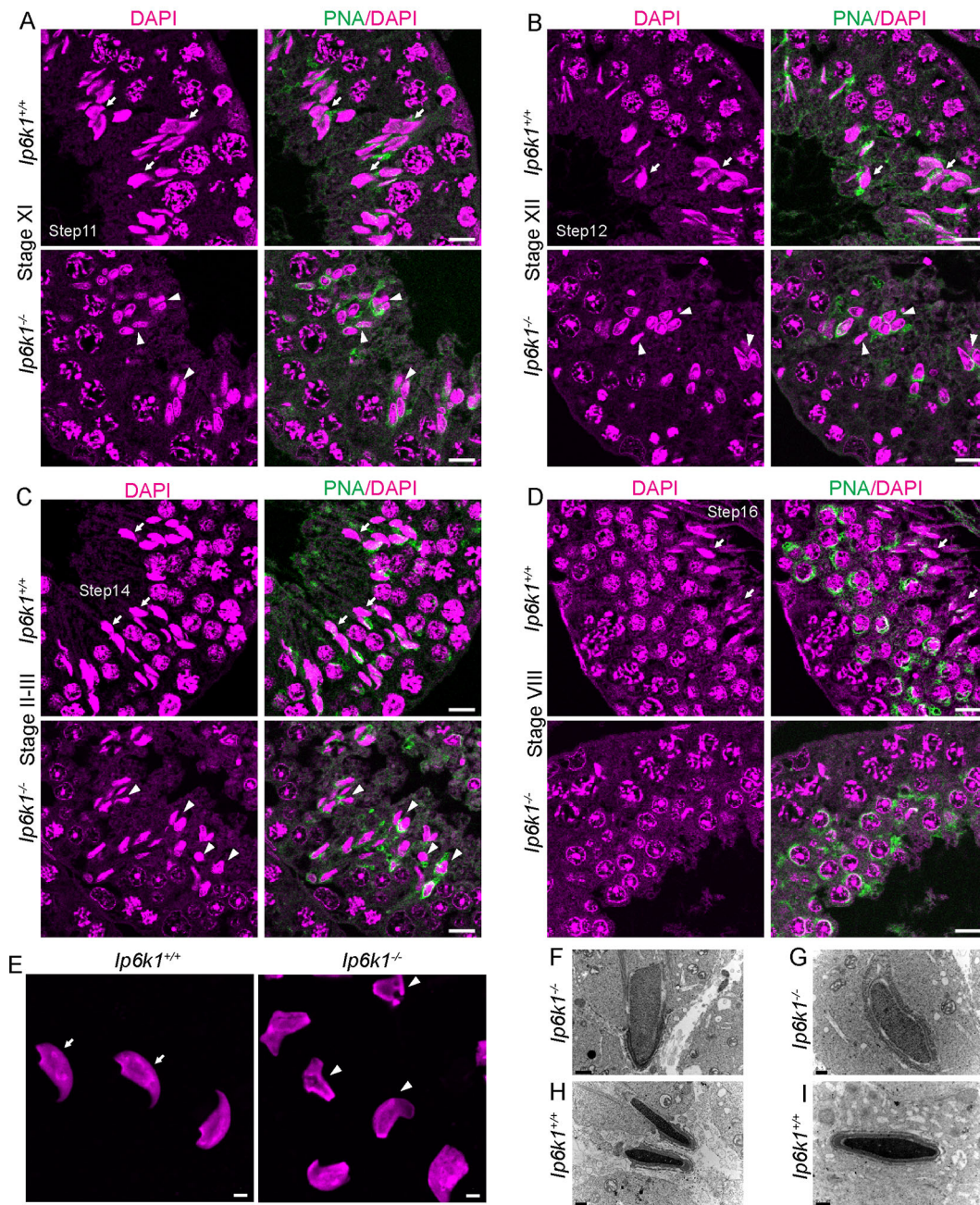


Fig. 3. Loss of IP6K1 leads to abnormal elongation and DNA condensation in mouse spermatids. (A–D) *Ip6k1*^{+/+} and *Ip6k1*^{-/-} testis cross-sections were stained with peanut agglutinin (PNA) to detect the outer acrosomal membrane, and DAPI to mark nuclei. The white regions indicate the overlap of PNA (green) and DAPI (magenta). The stage of the seminiferous epithelium was determined for each tubule cross-section by examining the presence, morphology and position of different cell types. Scale bar: 10 μm. The complete tubules are shown in Fig. S2. (A) Stage XI tubules – arrows indicate step 11 condensing spermatids in *Ip6k1*^{+/+} testes, and arrowheads point to abnormally condensing spermatids in *Ip6k1*^{-/-} testes. (B) Stage XII tubules – compared to step 12 *Ip6k1*^{+/+} spermatids (arrows), elongating spermatids in *Ip6k1*^{-/-} mice (arrowheads) undergo abnormal elongation and condensation. (C) Stage II–III tubules – arrows indicate step 14 spermatids in *Ip6k1*^{+/+} testes, and arrowheads indicate abnormal spermatids in *Ip6k1*^{-/-} testes. (D) Stage VIII tubules – fully condensed step 16 elongated spermatids (arrows) are present in *Ip6k1*^{+/+} testes but are absent in *Ip6k1*^{-/-} testes, which only contain round spermatids. (E) Dark zone elongated spermatids stained with DAPI (magenta) indicating spermatid head morphology. Arrows point to the typical hook-shape of dark zone elongated spermatids in *Ip6k1*^{+/+} mice and arrowheads indicate abnormally condensed elongated spermatids in *Ip6k1*^{-/-} mice. Scale bars: 2 μm. (F–I) TEM images of abnormally condensed and loosely packed *Ip6k1*^{-/-} elongated spermatids (F,G) and fully condensed and tightly packed *Ip6k1*^{+/+} elongated spermatids (H,I). Scale bars: 1 μm (F); 0.5 μm (G–I).

To follow the process of DNA condensation during spermiogenesis, we tracked the presence of histone H4 in *Ip6k1*^{+/+} and *Ip6k1*^{-/-} elongating spermatids (Fig. S4A–C). As expected, histone H4 was visible in both *Ip6k1*^{+/+} and *Ip6k1*^{-/-} step 10–11 (stage X/XI) early elongating spermatids (Fig. 4A). As *Ip6k1*^{+/+} spermatids advanced to step 12 (stage XII), histone H4 was no longer

visible, but *Ip6k1*^{-/-} spermatids in stage XII and II–IV tubules contained histone H4, suggesting that these spermatids do not progress beyond step 11 (Fig. 4B,C). Elongating spermatids in stage II–III *Ip6k1*^{-/-} tubules also stained positive for *in situ* TUNEL labelling, and showed the presence of cleaved caspase 3, suggesting that they undergo apoptosis and are eventually lost (Fig. 4D,E).

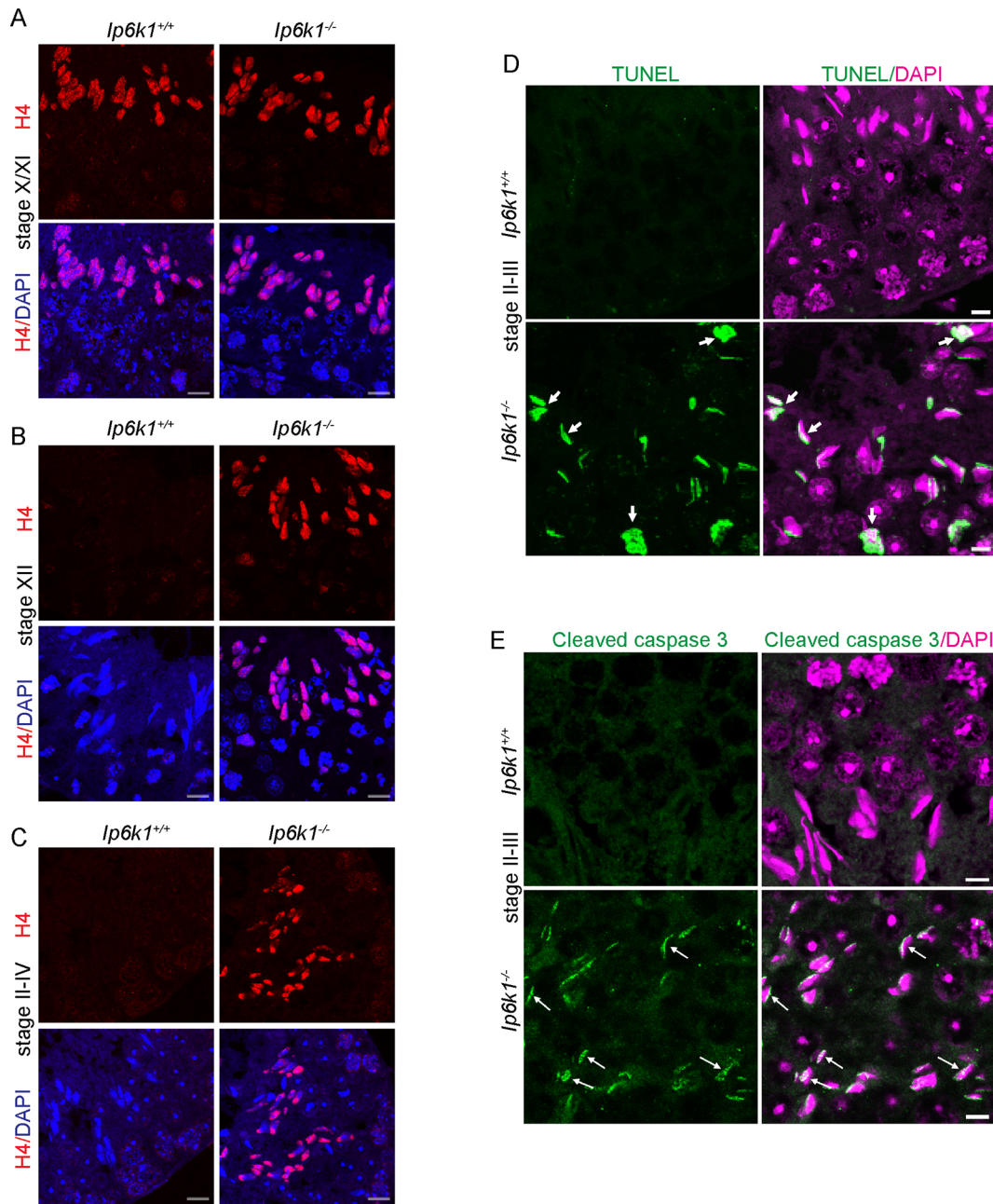


Fig. 4. Loss of IP6K1 leads to defective somatic histone removal and apoptosis in *Ip6k1*^{-/-} elongating spermatids. (A–C) Immunostaining of *Ip6k1*^{+/+} and *Ip6k1*^{-/-} testis sections shows abnormal retention of histone H4 (red) in *Ip6k1*^{-/-} elongating spermatids. Spermatid nuclei were counterstained with DAPI (blue). The complete tubules are shown in Fig. S4. Histone H4 is detected in step 10–11 (stage XIX) *Ip6k1*^{+/+} and *Ip6k1*^{-/-} elongating spermatids (A), is completely evicted in step 12 (stage XII) *Ip6k1*^{+/+} elongating spermatids (B), but is retained in *Ip6k1*^{-/-} spermatids in stage XII (B) and stage II–IV tubules (C). Scale bars: 10 μ m. (D) TUNEL (green) and DAPI (magenta) staining of stage II–III *Ip6k1*^{+/+} and *Ip6k1*^{-/-} testis cross-sections. Arrows indicate extensive DNA damage in *Ip6k1*^{-/-} elongating spermatids. White regions (overlap of magenta and green) indicate TUNEL-positive nuclei. Scale bars: 5 μ m. (E) Cleaved caspase 3 (green) staining in *Ip6k1*^{+/+} and *Ip6k1*^{-/-} testis cross-sections indicating apoptotic elongating spermatids (arrows) in *Ip6k1*^{-/-} testes. Spermatid nuclei were counterstained with DAPI (magenta). White regions (overlap of magenta and green) indicate cleaved caspase 3-positive nuclei. Scale bars: 5 μ m.

Loss of IP6K1 leads to disruption of chromatoid bodies

A close look at the pattern of expression of IP6K1 in round spermatids reveals that it is enriched in granules within the cytoplasm (Fig. 2Ciii). These granules are reminiscent of chromatoid bodies, which are perinuclear ribonucleoprotein complexes found in round spermatids at steps 1 through 8, and are involved in mRNA translational control, mRNA decay and small RNA-mediated gene regulation (Parvinen, 2005; Kotaja and Sassone-Corsi, 2007; Meikar et al., 2011). Co-staining of squash

preparations of *Ip6k1*^{+/+} round spermatids to detect IP6K1 and the chromatoid body marker protein MIWI (also known as PIWIL1) revealed that IP6K1 is indeed localised to the chromatoid body in round spermatids in addition to being present in the cytoplasm (Fig. 5A). We therefore examined the architectural integrity of the chromatoid body in *Ip6k1*^{+/+} and *Ip6k1*^{-/-} spermatids. On staining testis sections to detect MVH (also known as DDX4), an RNA helicase enriched in the chromatoid body, a conspicuous perinuclear spot was observed in *Ip6k1*^{+/+} round spermatids (Fig. 5B).

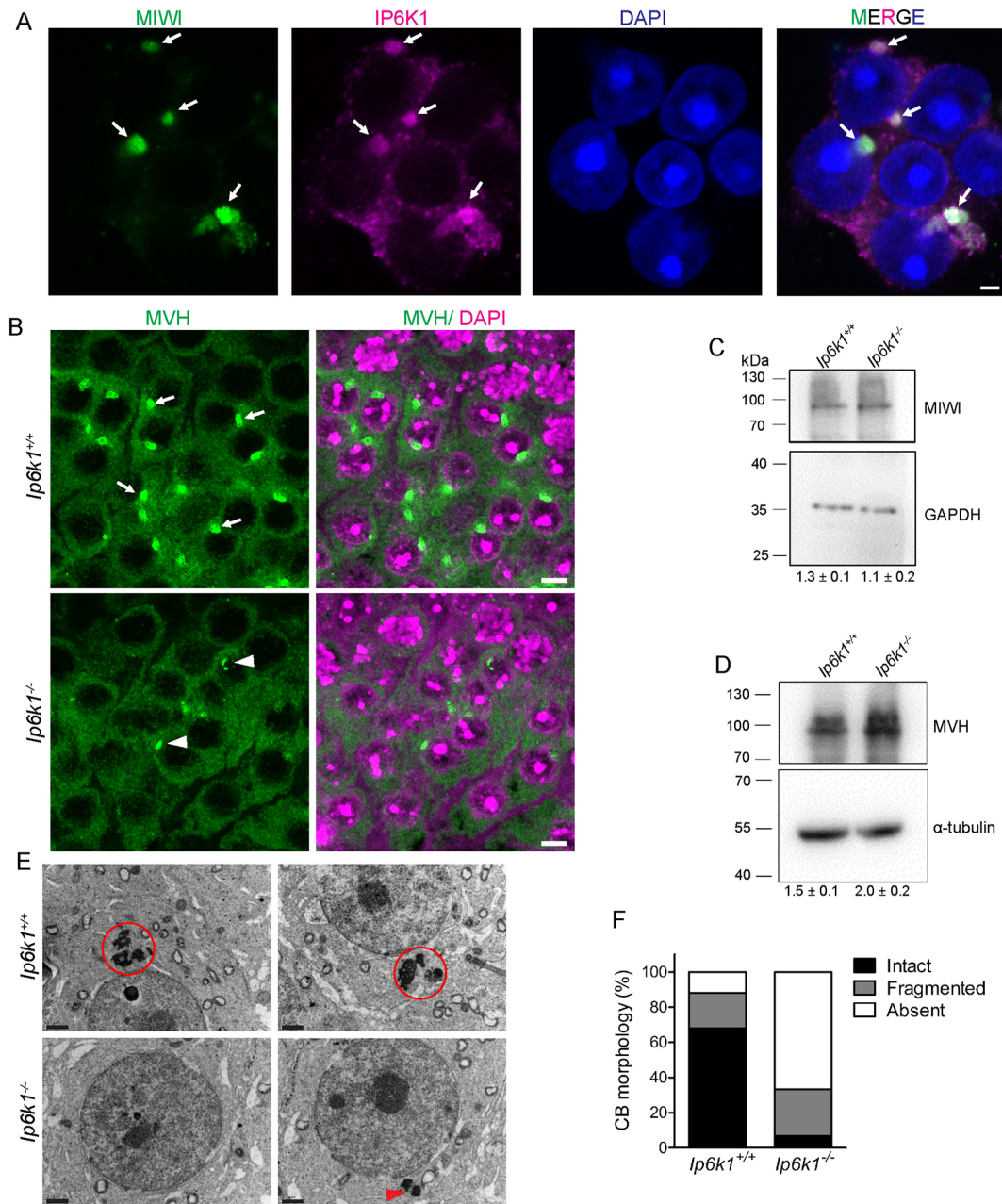


Fig. 5. IP6K1 localises to the chromatoid body and is essential for its assembly in round spermatids. (A) Immunostaining of round spermatid squash preparations shows colocalisation (white) of IP6K1 (magenta) with the chromatoid body marker MIWI (green) indicating that IP6K1 is present in the chromatoid body (arrows). Spermatid nuclei were counterstained with DAPI (blue). Scale bar: 2 µm. (B) Immunostaining of *Ip6k1*^{+/+} and *Ip6k1*^{-/-} testis sections to detect MVH (green), a protein enriched in chromatoid bodies. MVH is present in conspicuous perinuclear granules in *Ip6k1*^{+/+} round spermatids (arrows), whereas in *Ip6k1*^{-/-} round spermatids these MVH-rich granules are absent except for small spots around the nuclei in some cells (arrowheads). Nuclei were counterstained with DAPI (magenta). Scale bars: 5 µm. (C, D) Representative immunoblots of chromatoid body markers MIWI (C) and MVH (D) in whole testis extracts. GAPDH (C) or α-tubulin (D) were used as loading controls. The intensity of the chromatoid body protein normalised to the loading control is indicated as mean ± range from two independent experiments, showing that MIWI levels are unchanged, whereas MVH is marginally higher in *Ip6k1*^{-/-} than in *Ip6k1*^{+/+} testes. (E) Representative TEM images of round spermatids showing amorphous lobulated electron-dense chromatoid bodies in *Ip6k1*^{+/+} spermatids (encircled) and either no or fragmented (arrowhead) chromatoid bodies in *Ip6k1*^{-/-} spermatids. Scale bars: 1 µm. (F) Quantification of chromatoid body (CB) morphology from images in E. TEM images of *Ip6k1*^{+/+} (*n*=25) and *Ip6k1*^{-/-} (*n*=30) round spermatids were analysed to classify chromatoid body morphology as intact, fragmented or absent.

However, most *Ip6k1*^{-/-} spermatids did not show any chromatoid body staining, with some spermatids showing tiny fragmented spots (Fig. 5B). MVH and MIWI are the two most abundant proteins in the chromatoid body, constituting ~40% (mole percentage) of the chromatoid body proteome (Meikar et al., 2014). We noted that the protein level of MIWI is unaltered and that of MVH is marginally increased in *Ip6k1*^{-/-} testes, suggesting that the disruption of the

chromatoid body in *Ip6k1*^{-/-} mice is not due to reduced levels of these proteins (Fig. 5C,D). The ultrastructure of the chromatoid body was further examined by transmission electron microscopy. In contrast to massive sponge-like perinuclear aggregates observed in *Ip6k1*^{+/+} spermatids, *Ip6k1*^{-/-} spermatids showed altered chromatoid body morphologies (Fig. 5E). While a few *Ip6k1*^{-/-} spermatids contained an intact chromatoid body, in most of these

spermatids the chromatoid body was either fragmented or absent (Fig. 5F). These data demonstrate that IP6K1 has a critical function in the assembly of the chromatoid body, which in turn has been shown to be essential for normal spermatid development (Vasileva et al., 2009; Tanaka et al., 2011).

TNP2 and PRM2 are prematurely synthesised and aberrantly localised in the absence of IP6K1

The temporal regulation of sperm DNA condensation is dependent on the timely expression of transition proteins and protamines. The mRNAs encoding these proteins are transcribed in round spermatids, but are stored in a translationally repressed state to be translated during spermatid elongation (Kistler et al., 1996; Braun, 1998; Kleene, 2013). Translational control of mRNAs in round spermatids involves the interaction of cis-elements in the mRNA with RNA-binding proteins and microRNAs, and differs for individual mRNAs (Kleene, 2013). The role of the chromatoid body in translational repression of spermatid mRNAs has been debated (Parvinen, 2005; Kotaja and Sassone-Corsi, 2007; Kleene and Cullinane, 2011). mRNAs encoding TNP2 and PRM2 have been shown to localise to the chromatoid body (Saunders et al., 1992; Fukuda et al., 2013), and disruption of the chromatoid body has been shown to cause male infertility and can also lead to aberrant cytoplasmic aggregation of TNP2 and PRM2 (Reuter et al., 2011; Tanaka et al., 2011). It has previously been shown that *Prm2* mRNA is expressed in 28 dpp juvenile mouse testes, but significant levels of PRM2 protein can be detected only at 32 dpp (Fukuda et al., 2013). Therefore, to investigate whether the loss of the chromatoid body in *Ip6k1*^{-/-} spermatids leads to changes in TNP2 and PRM2 expression, we examined the levels of these proteins in 28- and 35-day-old juvenile testes. At 28 dpp, neither protein was detected in *Ip6k1*^{+/+} testes whereas *Ip6k1*^{-/-} testes showed premature expression of both these proteins (Fig. 6A,B). TNP2 and PRM2 expression was detected in both *Ip6k1*^{+/+} and *Ip6k1*^{-/-} 35 dpp testes, but protein levels were higher in knockout mice. In contrast to protein levels, there was either a decrease or no change in the levels of *Tnp2* and *Prm2* transcripts in 28 and 35 dpp *Ip6k1*^{-/-} compared with that seen in *Ip6k1*^{+/+} testes (Fig. 6C). This suggests that the premature expression of these proteins is not attributable to an increase in mRNA abundance, but instead is a result of derepression of their translational silencing. Testicular sections of 28 dpp mice revealed that TNP2 is highly expressed in the nuclei of a few abnormally condensed *Ip6k1*^{-/-} spermatids (Fig. 6D), and PRM2 is prematurely expressed in the nuclei of most of the *Ip6k1*^{-/-} round spermatids (Fig. 6E). In adult mice, PRM2 showed uniform nuclear staining in *Ip6k1*^{+/+} spermatids, but weak nuclear staining in some *Ip6k1*^{-/-} elongating spermatids and aberrant cytoplasmic localisation in the form of large aggregates around spermatid nuclei (Fig. 6F). The seminiferous tubules of 6-month-old *Ip6k1*^{-/-} mice harboured prematurely condensed round spermatids that were positive for expression of TNP2 and PRM2 (Fig. 6G). Similar patterns of aberrant TNP2 and PRM2 expression and localisation have been observed in *Miw1*- and *Tdrd6*-knockout mice, which exhibit defects in chromatoid body assembly (Reuter et al., 2011; Tanaka et al., 2011). Taken together, these data suggest that IP6K1 is essential for the post-transcriptional regulation of *Tnp2* and *Prm2* mRNA expression in round spermatids.

DISCUSSION

This study investigates the underlying basis of spermatogenic arrest in mice lacking the inositol phosphate kinase IP6K1. Our data show that IP6K1 is essential for histone removal and sperm head

elongation during spermatid differentiation. We show that IP6K1 is a novel and essential component of chromatoid bodies, which are either disintegrated or absent in round spermatids lacking IP6K1. We also observe premature translation of TNP2 and PRM2 in round spermatids of juvenile mice, and aberrant localisation of these proteins in adult mice, leading to abnormal DNA condensation in elongating spermatids (Fig. 7). These deformed elongating spermatids ultimately undergo apoptosis, which is responsible for azoospermia and male infertility in *Ip6k1*^{-/-} mice.

To date, IP6K1 is the only inositol polyphosphate metabolic enzyme shown to participate in mammalian gametogenesis. Another *Ip6k1* mutant mouse strain generated by gene trapping technology introduced a retroviral insertion between exons 2 and 3 (coding exons 1 and 2), resulting in the loss of *Ip6k1* transcript (<http://www.informatics.jax.org/allele/key/36801>). Preliminary histological analysis of these male mice revealed bilateral epididymal azoospermia and testicular degeneration, suggesting that they would display male sterility, similar to what we observe upon deletion of the terminal exon 6. Deletion of the other IP6K isoforms, IP6K2 and IP6K3, has no effect on spermatogenesis (Morrison et al., 2009; Fu et al., 2015; Moritoh et al., 2016), indicating that the different IP6K isoforms have non-overlapping functions in mammalian reproductive physiology. Treatment of mice with the pan-IP6K inhibitor TNP was shown to have no effect on male fertility, which was attributed to the inability of this drug to penetrate the blood–testis barrier (Ghoshal et al., 2016).

In mammals, the synthesis of 5-IP₇ relies on a cascade of metabolic enzymes, starting with the release of I(1,4,5)P₃ from phosphatidylinositol 4,5-bisphosphate [PI(4,5)P₂] (Fig. S4D). I(1,4,5)P₃ is converted into I(1,3,4,5)P₄ by inositol 1,4,5-trisphosphate 3-kinases (IP3Ks) of which there are three isoforms in mammals (Leyman et al., 2007). I(1,3,4,5)P₄ is subsequently converted into I(1,3,4,5,6)P₅ by inositol polyphosphate multikinase (IPMK) (Fujii and York, 2005), and I(1,3,4,5,6)P₅ is converted into IP₆ by inositol-pentakisphosphate 2-kinase (IPPK) (Verbsky et al., 2005a), both of which have only single isoforms in mammals. In an alternative pathway, I(1,3,4,5)P₄ is first dephosphorylated to I(1,3,4)P₃ and subsequently phosphorylated by ITPK1 to yield I(1,3,4,6)P₄, which is then phosphorylated to I(1,3,4,5,6)P₅ by IPMK (Verbsky et al., 2005b). Targeted mutant mice have been generated for all of the enzymes responsible for the synthesis of inositol phosphate precursors to 5-IP₇. Loss of any of the three IP3K isoforms did not alter viability or fertility in mice (Jun et al., 1998; Pouillon et al., 2003). However, mouse embryonic fibroblasts lacking all three IP3K isoforms have been shown to synthesise IP₄, IP₅ and IP₆, making use of a redundancy in the metabolic pathway that allows IPMK to take over the function of IP3Ks (Leyman et al., 2007) (Fig. S4D). A hypomorphic mutant for ITPK1 is viable and fertile (Wilson et al., 2009). Although the levels of inositol polyphosphates were not measured in cells derived from these mice, it is known that IPMK can catalyse the synthesis of I(1,3,4,5,6)P₅ from I(1,3,4,5)P₄ in mammalian cells, suggesting that ITPK1 is not essential for the synthesis of IP₆ (Fujii and York, 2005). Mice lacking IPMK die at around embryonic day 9.5, and cells derived from these embryos have negligible levels of IP₅ and IP₇, and an ~90% reduction in IP₆ (Frederick et al., 2005; Maag et al., 2011). Homozygous deletion of IPPK, the only enzyme responsible for IP₆ synthesis, led to early embryonic lethality and no embryos could be derived for inositol polyphosphate analysis (Verbsky et al., 2005a). IP₅ and IP₆ may have specific functions in spermatogenesis that are independent of their role as 5-IP₇ precursors. Male germ-cell-specific knockout mice for IPMK and IPPK will be required to

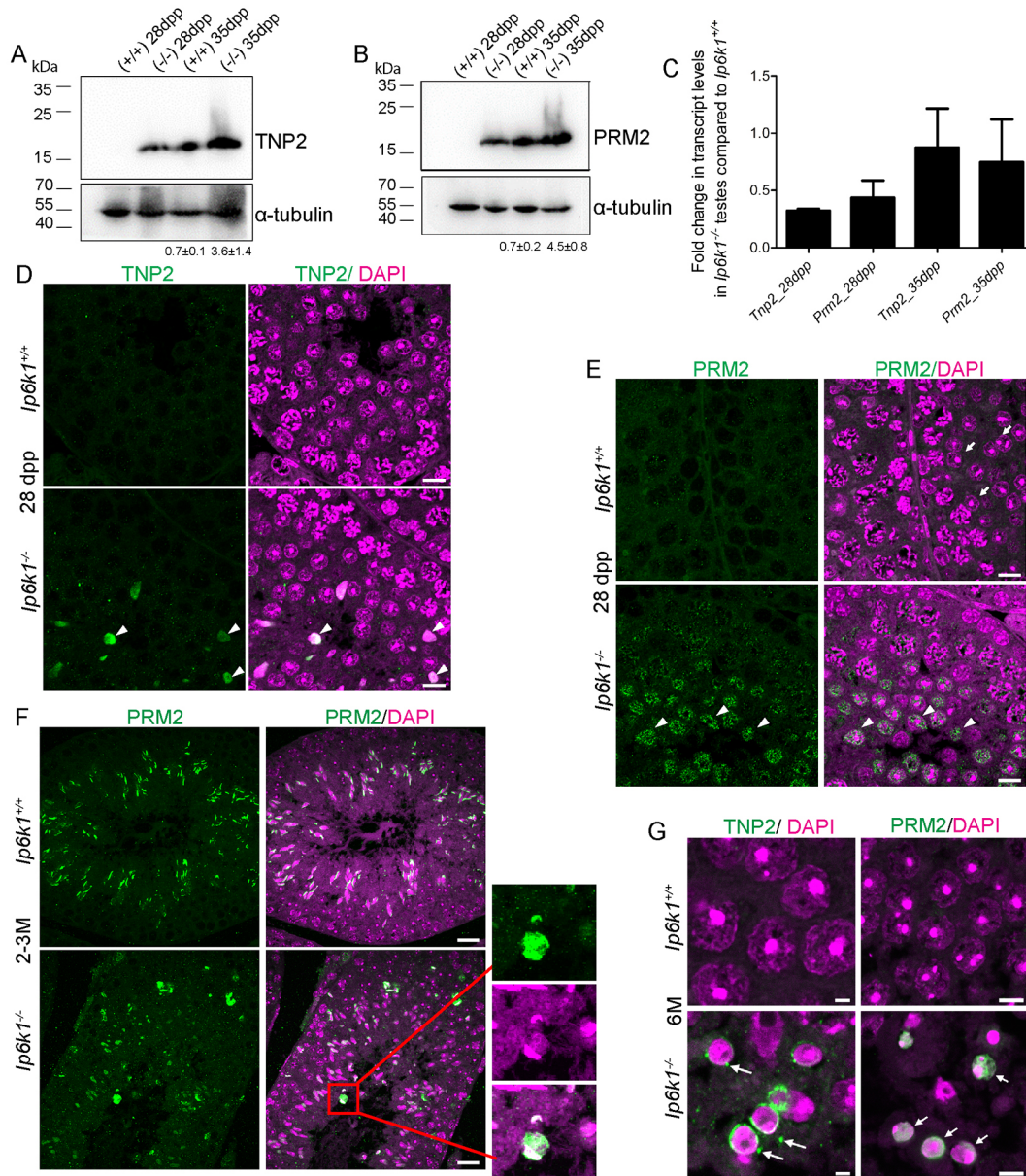


Fig. 6. IP6K1 prevents the premature translation of key spermiogenic genes. (A,B) Western blot analysis of TNP2 (A) and PRM2 (B) in 28 dpp and 35 dpp testes of *Ip6k1*^{+/+} (+/+) and *Ip6k1*^{-/-} (-/-) mice reveals premature expression of these proteins in 28 dpp *Ip6k1*^{-/-} testes. The levels of TNP2 or PRM2 in 35 dpp testes, normalised to the levels of the loading control (α -tubulin) are indicated as the mean \pm s.e.m. from three independent experiments. Both proteins were expressed at higher levels in *Ip6k1*^{-/-} testes. (C) RT-qPCR analysis of *Tnp2* and *Prm2* transcripts to estimate their levels in 28 dpp and 35 dpp *Ip6k1*^{+/+} and *Ip6k1*^{-/-} testes. The graph shows the fold change in transcript levels in *Ip6k1*^{-/-} testes compared to that in *Ip6k1*^{+/+} testes. Data represents the mean \pm range of two biological replicates (each calculated from the average of two or three technical replicates). (D) Immunostaining of *Ip6k1*^{+/+} and *Ip6k1*^{-/-} 28 dpp testis cross-sections to detect TNP2 (green). Nuclei are counterstained with DAPI (magenta). *Ip6k1*^{+/+} 28 dpp testes show no detectable TNP2 staining, whereas *Ip6k1*^{-/-} testes show premature translation of TNP2 in some abnormally shaped spermatids (arrowheads). Scale bars: 10 μ m. (E) Immunostaining of *Ip6k1*^{+/+} and *Ip6k1*^{-/-} 28 dpp testis cross-sections to detect PRM2 (green). Nuclei are counterstained with DAPI (magenta). PRM2 is prematurely translated in round spermatids of 28 dpp *Ip6k1*^{-/-} mice (arrowheads) but not present in *Ip6k1*^{+/+} round spermatids (arrows). Scale bars: 10 μ m. (F) Immunostaining of young adult (2–3 M; 2–3 M) testis cross-sections of *Ip6k1*^{+/+} and *Ip6k1*^{-/-} mice to detect PRM2 (green). Nuclei are counterstained with DAPI (magenta). In *Ip6k1*^{+/+} mice, PRM2 is recruited to DNA in elongating spermatids. In *Ip6k1*^{-/-} mice, some spermatids show nuclear PRM2, but PRM2 is predominantly seen as large aggregates around the spermatid nuclei (inset). Scale bars: 20 μ m. (G) Immunostaining of testes from 6-month-old (6 M) *Ip6k1*^{+/+} and *Ip6k1*^{-/-} mice to detect TNP2 or PRM2 (green). Nuclei are counterstained with DAPI (magenta). *Ip6k1*^{-/-} round spermatids (arrows) undergo early nuclear condensation due to prematurely synthesised TNP2 and PRM2. Scale bars: 2 μ m (TNP2), 5 μ m (PRM2). In D–G, white regions indicate the overlap of DAPI-stained nuclei (magenta) and TNP2 or PRM2 (green).

address this possibility. Since no knockout mice have been generated for the two mammalian PPIP5K isoforms that are responsible for the synthesis of IP₈ [1,5(PP)₂-IP₄] from 5-IP₇ (Fig. S4D), the importance of this inositol pyrophosphate in male gametogenesis is unknown.

Our most interesting finding is the identification of IP6K1 as a novel protein component of the chromatoid body. The expression pattern of IP6K1 in male germ cells resembles that of other integral chromatoid body components such as MIWI and the tudor domain-containing proteins TDRD6 and TDRD7. These proteins, like

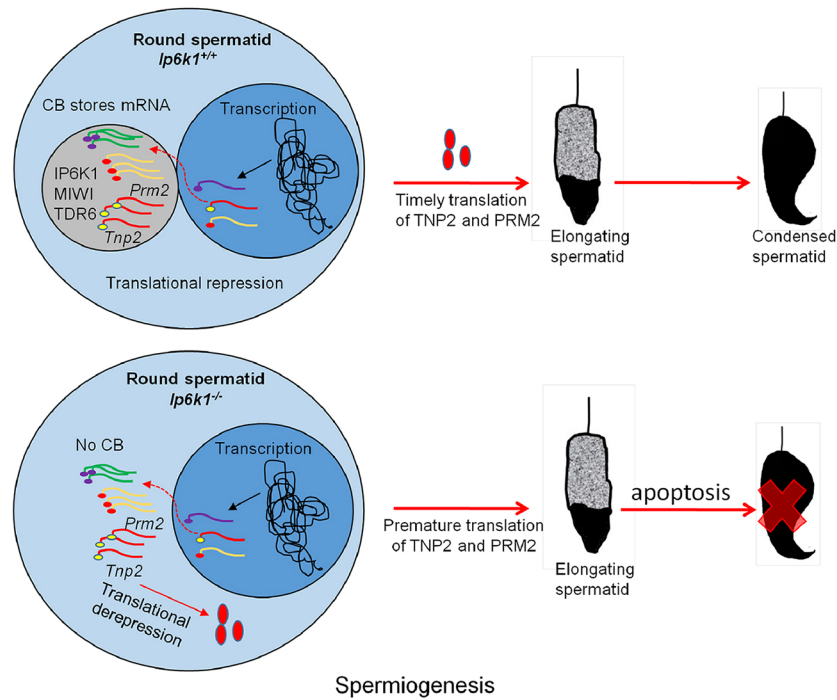


Fig. 7. IP6K1 is essential for spermiogenesis. During spermiogenesis, IP6K1 is required for assembly of chromatoid bodies (CB), and the storage of *Tnp2* and *Prm2* transcripts in a repressed state. In the absence of IP6K1, there is a loss of chromatoid bodies in round spermatids, and translational derepression of *Tnp2* and *Prm2*, resulting in arrested spermiogenesis.

IP6K1, are highly expressed in the cytoplasm of late pachytene cells and continue to be expressed at high levels in the cytoplasm and chromatoid body of round spermatids (Deng and Lin, 2002; Vasileva et al., 2009; Tanaka et al., 2011). The loss of TDRD6 or TDRD7, which regulate ribonucleoprotein remodelling in chromatoid bodies, leads to male-specific sterility due to abnormalities in chromatoid body formation (Vasileva et al., 2009; Tanaka et al., 2011). Loss of the MIWI RNase activity has been shown to result in a similar pattern of PRM2 aggregation around elongating spermatids to that we observed in *Ip6k1*^{-/-} mice (Reuter et al., 2011).

Precise timing and levels of transition protein and protamine expression are important for the progression of spermiogenesis, and premature translation of these proteins can lead to spermiogenic defects similar to those observed in *Ip6k1*^{-/-} mice (Lee et al., 1995; Tsenden et al., 2007; Fukuda et al., 2013). Transgenic mice carrying *Tnp2* with a modified 3' untranslated region (UTR) that causes its premature expression in round spermatids display abnormal sperm head morphology and male infertility (Tsenden et al., 2007). Mice lacking CBF-A (also known as HNRNPAB), an RNA-binding protein involved in temporal regulation of *Prm2* translation, display precocious translation of PRM2 leading to premature chromatin condensation in a subset of elongating spermatids (Fukuda et al., 2013). Transcripts encoding TNP2 and PRM2 have been shown to localise to the chromatoid body in step 7–8 round spermatids (Saunders et al., 1992; Fukuda et al., 2013), but, to our knowledge, there are no studies examining whether disruption of the chromatoid body alters the post-transcriptional regulation of these transcripts. Our data reveals that chromatoid body disruption associated with loss of IP6K1 correlates with premature translation of *Tnp2* and *Prm2*, suggesting that the chromatoid body localisation of these transcripts may be directly relevant to their translational repression. IP6K1 may also indirectly regulate translation of these transcripts independently of its involvement in chromatoid body formation.

It has been reported that *Ip6k1* transcripts rank second amongst the top five most abundant transcripts in the chromatoid body,

alongside transition proteins and protamines (Meikar et al., 2014). In the same study, functional classification of 88 chromatoid body-associated proteins revealed that they are predominantly involved in RNA binding and other RNA regulatory functions. IP6K1, on the other hand, is an inositol phosphate kinase, and possesses no obvious RNA-interacting regions. It is possible that 5-IP₇ synthesised by IP6K1 may be essential for the function of one or more chromatoid body proteins. Alternatively, IP6K1 may act independently of its catalytic activity as a scaffold protein to maintain architectural integrity of the chromatoid body.

MATERIALS AND METHODS

Mice

All animal experiments were performed in compliance with guidelines provided by the Committee for the Purpose of Control and Supervision of Experiments on Animals, Ministry of Environment, Forest, and Climate Change, Government of India. All animal experiments were approved by the Institutional Animal Ethics Committee (Protocol number PCD/CDFD/02 – version 2). Mice (*Mus musculus*, strain C57BL/6) used for this study were housed in the Centre for DNA Fingerprinting and Diagnostics animal facility located within the premises of Vimta Labs, Hyderabad. The *Ip6k1* gene knockout mouse was generated as previously described (Bhandari et al., 2008). This mouse carries a deletion spanning the splice site, coding region and a portion of the 3' UTR of the terminal exon (exon 6) of *Ip6k1*. *Ip6k1*^{+/+} and *Ip6k1*^{-/-} littermates were produced by breeding *Ip6k1*^{+/-} mice. Age-matched juvenile and adult 8- to 16-week-old male mice were used for the collection of testes. Images shown in the figures are representative of single experiments, but each experiment was repeated with *n*=3–5 *Ip6k1*^{+/+} and *Ip6k1*^{-/-} mice, and similar results were obtained. The number of animals used to obtain quantitative data (*n*) is indicated in the figure legends. Data were graphed and statistical analyses were performed as indicated in the figure legends, using GraphPad Prism 5. Statistical significance was defined as *P*<0.05.

Reagents and antibodies

All chemicals were purchased from Sigma-Aldrich, unless otherwise specified. Primary antibodies and their respective dilutions used for immunofluorescence (IF) and immunoblotting (IB) were: anti-TNP2

(Santa Cruz Biotechnology, sc21106; 1:200 IF, 1:500 IB); anti-PRM2 (Santa Cruz Biotechnology, sc-23104; 1:200 IF, 1:500 IB); anti-IP6K1 (Sigma-Aldrich, HPA040825; 1:300 IF), anti-IP6K1 (Santa Cruz Biotechnology, sc-10419; 1:500 IB); anti-cleaved caspase 3 (Cell Signaling Technology, 9661; 1:400 IF); anti-histone H4 (Abcam, ab10158; 1:300 IF); anti-MIWI (Santa Cruz Biotechnology, sc-22685; 1:200 IF, 1:500 IB); anti-MVH (Abcam, ab13840; 1:300 IF, 1:1000 IB); anti- α -tubulin (Sigma-Aldrich, T9025; 1:500 IF, 1:5000 IB); and anti-GAPDH (Sigma-Aldrich, G8795; 1:5000 IB) antibodies. Alexa Fluor 594-conjugated PNA lectin (Molecular Probes, L32459) was used at a dilution of 1:500.

Epididymal spermatozoa counting

Epididymides were dissected and collected in Dulbecco's modified Eagle's medium, cut into pieces and flushed out to release spermatozoa. These were filtered through a 40 μ m mesh to remove debris. The resuspended spermatozoa were then counted with a haemocytometer under a light microscope according to standard protocols.

Testosterone measurement

Blood collected from the retro-orbital sinus of *Ip6kl^{+/+}* and *Ip6kl^{-/-}* male mice was allowed to clot for 1 h at room temperature. The clots were centrifuged at 1100 *g* for 30 min at 4°C. Serum samples were collected and stored in sealed tubes at -80°C until assayed. Serum testosterone concentration was measured using an enzyme-linked immunosorbent assay (Enzo Life Sciences; ADI-900-065), following the manufacturer's guidelines. Serum samples diluted (1:10) in assay buffer were assayed in duplicate. The cross-reactivity of this assay is 14.6% for 19-hydroxytestosterone and 7.2% for androstenedione, but less than 1% for any other hormone or metabolite.

Histology

Ip6kl^{+/+} and *Ip6kl^{-/-}* male mice of different age groups were euthanised by carbon dioxide inhalation, and the testes and epididymides were dissected. After isolation, testes and epididymides were briefly washed with phosphate-buffered saline (PBS) and fixed in Bouin's solution for 48 h at 4°C. To remove the last traces of fixative, samples were washed in 70% ethanol, dehydrated, and embedded in paraffin wax. 4 μ m sections were prepared on glass slides, cleared in xylene and dehydrated in a graded series of ethanol. The sections were then stained with haematoxylin and eosin. Images were acquired with a bright-field light microscope (Nikon ECLIPSE Ni-U, NIS Elements acquisition software, 20 \times 0.5 N.A. or 40 \times 0.75 N.A. objectives). Stages of the seminiferous epithelia were identified according to established methods (Russell et al., 1990; Ahmed and de Rooij, 2009). *Ip6kl^{-/-}* sections were staged based on cells other than elongating or elongated spermatids.

Immunohistochemistry

Paraffin-embedded testis sections were deparaffinised in xylene, dehydrated in a graded ethanol series, boiled in 10 mM sodium citrate buffer (pH 6) in a microwave oven for 20 min to retrieve the antigen, washed in PBS, permeabilised in 0.5% Triton X-100 for 10 min, blocked in blocking buffer (5% BSA+0.1% Triton X-100 or 4% FBS+0.1% Triton X-100) for 1 h at room temperature (RT) and then incubated overnight at 4°C with primary antibodies diluted in blocking buffer. The slides were washed with PBS and stained with fluorophore-conjugated secondary antibodies, including Alexa Fluor 488-conjugated or Alexa Fluor 568-conjugated goat anti-rabbit-IgG (Molecular Probes), Alexa Fluor 488-conjugated goat anti-mouse-IgG (Molecular Probes), Alexa Fluor 488-conjugated donkey anti-goat-IgG (Santa Cruz Biotechnology) and Alexa Fluor 555-conjugated donkey anti-rabbit-IgG (Santa Cruz Biotechnology). All secondary antibodies were used at 1:500 dilution in blocking buffer and incubated at RT for 1 h. Finally, the slides were mounted in antifade mounting medium containing DAPI (H-1200, Vector Labs). Images were acquired with an LSM 510 (LSM acquisition software) or LSM 700 (Zen acquisition software) confocal microscope (Zeiss) equipped with 405, 488, 555/561 nm and two-photon lasers, and fitted with a 63 \times 1.4 NA objective.

TUNEL staining was performed using an APO-BrdUTM TUNEL assay kit (Sigma-Aldrich, A35125) according to the manufacturer's instructions. Briefly, testis sections were deparaffinised as described above and then labelled with BrdU in the presence of terminal deoxynucleotidyl transferase (TdT) enzyme for 2 h at 37°C. After two washes, the sections were incubated with Alexa Fluor 488-conjugated anti-BrdU antibody supplied with the kit for 1 h at RT. The slides were mounted and imaged as described above.

Western blotting

Testes from *Ip6kl^{+/+}* and *Ip6kl^{-/-}* male mice were dissected and briefly washed in chilled 1 \times PBS. Tunica albuginea were removed and seminiferous tubules were minced and collected in RIPA buffer (50 mM Tris-HCl pH 7.4, 150 mM NaCl, 1% Triton X-100, 0.5% sodium deoxycholate, 0.1% SDS, 1 mM EDTA, 10 mM NaF, 1 mM PMSF) containing freshly added protease inhibitor cocktail (Sigma-Aldrich). The tissues were subjected to homogenisation (D-1 Homogenizer-Dispenser, Micra) and sonication (Bioruptor, Diagenode). The extracts were centrifuged at 20,000 *g* for 15 min at 4°C and supernatants were immediately mixed with 4 \times SDS sample buffer to a final dilution of 1 \times . The samples were heated at 95°C for 5 min, resolved by SDS-PAGE and transferred onto PVDF membranes (GE Healthcare). Western blotting was performed to detect the protein of interest and to assess equal gel loading by sequential probing of blots with experimental and control antibodies. Alternatively, when the difference in size between the experimental and control proteins was significant, a blot corresponding to the same gel was cut and probed in parallel. Membranes were blocked with 5% skimmed milk for 1 h at RT, followed by incubation with the primary antibody overnight at 4°C. After washing three times with TBST buffer (20 mM Tris-HCl pH 7.6, 150 mM NaCl and 0.1% Tween 20), membranes were incubated at RT for 1 h with HRP-conjugated secondary antibodies as follows: goat anti-rabbit IgG conjugated to HRP (Southern Biotech, 4010-05; 1:5000) for MVH and GAPDH; donkey anti-goat IgG conjugated to HRP (Santa Cruz, sc2020; 1:3000) for IP6K1, TNP2, PRM2 and MIWI; and goat anti-mouse IgG conjugated to HRP (Southern Biotech, 1031-05; 1:10,000) for α -tubulin. After washing the membrane three times with TBST, specific proteins bands were detected using a chemiluminescence reagent (ECL Prime, GE Healthcare). Chemiluminescence was detected using the FlourChem E (Protein Simple) documentation system. Where required, blots were stripped using Restore™ Western Blot Stripping Buffer (ThermoFisher Scientific), and re-probed with the control antibody. Densitometry analysis of bands was performed by using ImageJ software (Fiji) or the multiplex band analysis tool in AlphaView software (Protein Simple). The band intensity of the protein of interest was normalised to the loading control.

Transmission electron microscopy

Transmission electron microscopy (TEM) was performed as previously reported (Chemes, 2013). All reagents used for TEM were obtained from Electron Microscopy Sciences unless specified otherwise. Testes from adult mice were excised and directly fixed in 4% glutaraldehyde in sodium cacodylate buffer (0.1 M, pH 7.4). After washing in a fresh solution of 4% glutaraldehyde, testes were cut into smaller pieces (0.5–1 mm) and then immersed in the same fixative for 3 h at RT. After washing with sodium cacodylate buffer, the tissues were again fixed in 2% osmium tetroxide for 3 h at RT. The testis pieces were then dehydrated through a graded series of ethanol (50, 70 and 96%) at 4°C. To achieve complete dehydration, tissues were immersed in 100% ethanol (three changes, 20 min each) followed by propylene oxide (three changes, 20 min each) at RT. After dehydration, tissues were initially infiltrated with a 1:1 mixture of propylene oxide and Embed-Araldite mix [1:1:3 mix of Embed 812:Araldite 502:dodecyl succinic anhydride (DDSA)] containing 3% BDMP-30 for 2 h at RT and then treated with only Embed-Araldite mix at RT (two changes for 3 h each and one change overnight). Tissue blocks were finally polymerised in Embed-Araldite mix at 60°C for 72 h. Ultra-thin sections were cut on an ultra-microtome (Leica) and mounted on 200-mesh uncoated copper grids (Ted Pella Inc.). Sections were stained with 2% uranyl acetate replacement stain for 1 h and 0.5% lead citrate in distilled water for 30 min. The observations were performed with a Tecnai G2 Spirit BioTWIN transmission electron microscope (FEI).

Isolation of elongated spermatids from seminiferous tubules

The procedure followed was similar to that described earlier (Kotaja et al., 2004). 8-week-old male mice were euthanised as described above, and testes were removed and decapsulated and seminiferous tubules transferred to a Petri dish containing PBS. When viewed under a transilluminating dissection microscope, seminiferous tubules produce different patterns of light absorption giving four different regions; weak spot (stages XII–I), strong spot (stages II–VI), dark zone (stages VII–VIII) and pale zone (stages IX–XI). The dark zone containing elongated spermatids was cut into 1 mm-long pieces and placed in 50 μ l of 100 mM sucrose. Elongated spermatids were obtained in suspension by gentle pipetting of the minced tissue for 1 min. Cells were dried on slides pre-dipped in 1% PFA containing 0.15% Triton X-100. Since dark zones were not clearly visible in *Ip6k1*^{-/-} tubules, cells in the region between the strong spot and pale zone were isolated and analysed. The dried slides were briefly washed in PBS followed by cell fixation in 4% PFA for 10 min, and mounted in antifade mounting medium containing DAPI (H-1200, Vector Labs). Images were acquired using an LSM 700 confocal microscope (Zeiss; Zen acquisition software; 405 nm laser) using a 63 \times 1.4 NA objective.

Real-time quantitative PCR

Quantification of mRNA levels was carried out by reverse transcription real-time quantitative PCR (RT-qPCR). Briefly, total cellular RNA was isolated from 28 dpp and 35 dpp *Ip6k1*^{+/+} and *Ip6k1*^{-/-} testes by using TRIzol reagent (Invitrogen) followed by a RNeasy Mini Kit (Qiagen) according to the manufacturers' instructions. 2 μ g RNA was used for first-strand cDNA synthesis by reverse transcription with SuperScript Reverse Transcriptase III (Invitrogen) and oligonucleotide dT primers. qPCR was performed using gene-specific primers on the ABI 7500 real-time PCR system (Applied Biosystems) with MESA GREEN qPCR MasterMix Plus for SYBR® Assay Low ROX (Eurogentec) for detection. All samples were run in two or three technical replicates. The sequences of primers used were: *Tnp2* forward, 5'-GCTCAGGGCGAAGATACAAGTG-3' and reverse, 5'-TGT-GACATCATCCCAACAGTCC-3'; *Pgm2* forward, 5'-GTAGGAGGCAC-CATCACTAAGC-3' and reverse, 5'-AGACATCGACATGGAATGGTG-3'; and *Gapdh* forward, 5'-GGAGAAGCCGGGGCCCACTTGAA-3' and reverse: 5'-GCATGGACTGTGGTCATGAGCCCTTCAC-3'. The difference in transcript levels was calculated using the fold change ($\Delta\Delta C_t$ method) (Schmittgen and Livak, 2008). ΔC_t is the C_t value for the gene of interest normalised to the C_t value of the respective *Gapdh* control in both *Ip6k1*^{+/+} and *Ip6k1*^{-/-} testes. $\Delta\Delta C_t$ values were calculated as a relative change in ΔC_t of the target gene in *Ip6k1*^{-/-} with respect to *Ip6k1*^{+/+} testes. Fold changes were expressed as $2^{-\Delta\Delta C_t}$.

Preparation of testicular cells for flow cytometry

Flow cytometry analysis of testicular cells was performed as described previously (Krishnamurthy et al., 2000). Testes were dissected, the tunica albuginea was removed, and the seminiferous tubules were minced in Ca²⁺- and Mg²⁺-free PBS (Gibco). Cells were dispersed by gentle aspiration, filtered using a 40 μ m nylon filter, and washed in PBS by centrifuging at 800 g for 5 min. The cells were re-suspended in PBS, fixed in 70% chilled ethanol, and stored at 4°C for 24 h or at -20°C for up to 1 week until further analysis. 1 \times 10⁶–2 \times 10⁶ ethanol-fixed testicular cells were washed with PBS and treated with 0.25% pepsin solution for 10 min at 37°C. Finally, cells were stained with propidium iodide (PI) staining solution (25 μ g/ml PI, 40 mg/ml RNase and 0.03% Nonidet P-40 in PBS) at RT for 20 min. The PI-stained cells were analysed on an Accuri C6 flow cytometer (BD Biosciences; excitation 488 nm; emission 585/40 nm).

Acknowledgements

We sincerely thank Dr Solomon Snyder at the Johns Hopkins University School of Medicine for the gift of *Ip6k1*^{+/+} mice. We acknowledge the infrastructure and staff of the CDFD experimental animal facility, especially Suman Komjeti, Jayant P. Hole and Sridhar Kavela for help with breeding and maintenance of mice. Renu Pasricha and H. Krishnamurthy at the Centre for Cellular and Molecular Platforms (C-CAMP), Bangalore, are thanked for assistance in TEM imaging and discussions on flow cytometry, respectively. We acknowledge the assistance of Joy P. Vallentyne and A. L. Annapurna with confocal imaging. We are very grateful to Manasa Chanduri and Sitalakshmi Thampatty for manuscript proofreading and

helpful suggestions. We thank all members of the Laboratory of Cellular Signalling for helpful comments.

Competing interests

The authors declare no competing or financial interests.

Author contributions

Conceptualization: A.B.M., R.B.; Methodology: A.B.M.; Validation: A.B.M.; Formal analysis: A.B.M., R.B.; Investigation: A.B.M.; Resources: R.B.; Data curation: A.B.M.; Writing - original draft: A.B.M., R.B.; Writing - review & editing: A.B.M., R.B.; Visualization: A.B.M.; Supervision: R.B.; Project administration: R.B.; Funding acquisition: R.B.

Funding

This work was supported by core funds from the Centre for DNA Fingerprinting and Diagnostics (CDFD), which is supported by the Department of Biotechnology, Ministry of Science and Technology, Government of India. A.B.M. is a recipient of Junior and Senior Research Fellowships of the University Grants Commission, Government of India.

Supplementary information

Supplementary information available online at <http://jcs.biologists.org/lookup/doi/10.1242/jcs.204966.supplemental>

References

- Ahmed, E. A. and de Rooij, D. G. (2009). Staging of mouse seminiferous tubule cross-sections. *Methods Mol. Biol.* **558**, 263–277.
- Aviles, M., Castells, M. T., Martinez-Menarguez, J. A., Abascal, I. and Ballesta, J. (1997). Localization of penultimate carbohydrate residues in zona pellucida and acrosomes by means of lectin cytochemistry and enzymatic treatments. *Histochem. J.* **29**, 583–592.
- Bellvé, A. R., Cavicchia, J. C., Millette, C. F., O'Brien, D. A., Bhatnagar, Y. M. and Dym, M. (1977). Spermatogenic cells of the prepubertal mouse. Isolation and morphological characterization. *J. Cell Biol.* **74**, 68–85.
- Bhandari, R., Juluri, K. R., Resnick, A. C. and Snyder, S. H. (2008). Gene deletion of inositol hexakisphosphate kinase 1 reveals inositol pyrophosphate regulation of insulin secretion, growth, and spermiogenesis. *Proc. Natl. Acad. Sci. USA* **105**, 2349–2353.
- Braun, R. E. (1998). Post-transcriptional control of gene expression during spermatogenesis. *Semin. Cell Dev. Biol.* **9**, 483–489.
- Chemes, H. E. (2013). Ultrastructural analysis of testicular tissue and sperm by transmission and scanning electron microscopy. *Methods Mol. Biol.* **927**, 321–348.
- Deng, W. and Lin, H. (2002). *miwi*, a murine homolog of *piwi*, encodes a cytoplasmic protein essential for spermatogenesis. *Dev. Cell.* **2**, 819–830.
- Frederick, J. P., Mattis, D., Wofford, J. A., Megosh, L. C., Drake, L. Y., Chiou, S.-T., Hogan, B. L. M. and York, J. D. (2005). An essential role for an inositol polyphosphate multikinase, *lpk2*, in mouse embryogenesis and second messenger production. *Proc. Natl. Acad. Sci. USA* **102**, 8454–8459.
- Fu, C., Xu, J., Li, R.-J. and Crawford, J. A. (2015). Inositol hexakisphosphate kinase-3 regulates the morphology and synapse formation of cerebellar purkinje cells via spectrin/adducin. *J. Neurosci.* **35**, 11056–11067.
- Fujii, M. and York, J. D. (2005). A role for rat inositol polyphosphate kinases *rlpk2* and *rlpk1* in inositol pentakisphosphate and inositol hexakisphosphate production in rat-1 cells. *J. Biol. Chem.* **280**, 1156–1164.
- Fukuda, N., Fukuda, T., Sinnamon, J., Hernandez-Hernandez, A., Izadi, M., Raju, C. S., Czaplinski, K. and Percipalle, P. (2013). The transacting factor CBF-A/Hnmpab binds to the A2RE/RTS element of protamine 2 mRNA and contributes to its translational regulation during mouse spermatogenesis. *PLoS Genet.* **9**, e1003858.
- Ghoshal, S., Zhu, Q., Asteian, A., Lin, H., Xu, H., Ernst, G., Barrow, J. C., Xu, B., Cameron, M. D., Kamenecka, T. M. et al. (2016). TNP [N2-(m-Trifluorobenzyl), N6-(p-nitrobenzyl)purine] ameliorates diet induced obesity and insulin resistance via inhibition of the IP6K1 pathway. *Mol. Metab.* **5**, 903–917.
- Jun, K., Choi, G., Yang, S. G., Choi, K. Y., Kim, H., Chan, G. C. K., Storm, D. R., Albert, C., Mayr, G. W., Lee, C. J. et al. (1998). Enhanced hippocampal CA1 LTP but normal spatial learning in inositol 1,4,5-trisphosphate 3-kinase(A)-deficient mice. *Learn Mem.* **5**, 317–330.
- Kierszenbaum, A. L., Rivkin, E. and Tres, L. L. (2007). Molecular biology of sperm head shaping. *Soc. Reprod. Fertil. Suppl.* **65**, 33–43.
- Kistler, W. S., Henriksen, K., Mali, P. and Parvonen, M. (1996). Sequential expression of nucleoproteins during rat spermiogenesis. *Exp. Cell Res.* **225**, 374–381.
- Kleene, K. C. (2013). Connecting cis-elements and trans-factors with mechanisms of developmental regulation of mRNA translation in meiotic and haploid mammalian spermatogenic cells. *Reproduction* **146**, R1–R19.

- Kleene, K. C. and Cullinane, D. L. (2011). Maybe repressed mRNAs are not stored in the chromatoid body in mammalian spermatids. *Reproduction* **142**, 383–388.
- Kluin, P. M., Kramer, M. F. and de Rooij, D. G. (1982). Spermatogenesis in the immature mouse proceeds faster than in the adult. *Int. J. Androl.* **5**, 282–294.
- Kotaja, N. and Sassone-Corsi, P. (2007). The chromatoid body: a germ-cell-specific RNA-processing centre. *Nat. Rev. Mol. Cell Biol.* **8**, 85–90.
- Kotaja, N., Kimmins, S., Brancorsini, S., Hentsch, D., Vonesch, J.-L., Davidson, I., Parvinen, M. and Sassone-Corsi, P. (2004). Preparation, isolation and characterization of stage-specific spermatogenic cells for cellular and molecular analysis. *Nat. Methods* **1**, 249–254.
- Krishnamurthy, H., Danilovich, N., Morales, C. R. and Sairam, M. R. (2000). Qualitative and quantitative decline in spermatogenesis of the follicle-stimulating hormone receptor knockout (FORKO) mouse. *Biol. Reprod.* **62**, 1146–1159.
- Lee, K., Haugen, H. S., Clegg, C. H. and Braun, R. E. (1995). Premature translation of protamine 1 mRNA causes precocious nuclear condensation and arrests spermatid differentiation in mice. *Proc. Natl. Acad. Sci. USA* **92**, 12451–12455.
- Leyman, A., Pouillon, V., Bostan, A., Schurmans, S., Erneux, C. and Pesesse, X. (2007). The absence of expression of the three isoenzymes of the inositol 1,4,5-trisphosphate 3-kinase does not prevent the formation of inositol pentakisphosphate and hexakisphosphate in mouse embryonic fibroblasts. *Cell Signal.* **19**, 1497–1504.
- Luria, A., Morisseau, C., Tsai, H.-J., Yang, J., Inceoglu, B., De Taeye, B., Watkins, S. M., Wiest, M. M., German, J. B. and Hammock, B. D. (2009). Alteration in plasma testosterone levels in male mice lacking soluble epoxide hydrolase. *Am. J. Physiol. Endocrinol. Metab.* **297**, E375–E383.
- Maag, D., Maxwell, M. J., Hardesty, D. A., Boucher, K. L., Choudhari, N., Hanno, A. G., Ma, J. F., Snowman, A. S., Pietropaoli, J. W., Xu, R. et al. (2011). Inositol polyphosphate multikinase is a physiologic PI3-kinase that activates Akt/PKB. *Proc. Natl. Acad. Sci. USA* **108**, 1391–1396.
- Meikar, O., Da Ros, M., Korhonen, H. and Kotaja, N. (2011). Chromatoid body and small RNAs in male germ cells. *Reproduction* **142**, 195–209.
- Meikar, O., Vagin, V. V., Chalmel, F., Sostar, K., Lardenois, A., Hammell, M., Jin, Y., Da Ros, M., Wasik, K. A., Toppari, J. et al. (2014). An atlas of chromatoid body components. *RNA* **20**, 483–495.
- Moritoh, Y., Oka, M., Yasuhara, Y., Hozumi, H., Iwachidow, K., Fuse, H. and Tozawa, R. (2016). Inositol hexakisphosphate kinase 3 regulates metabolism and lifespan in mice. *Sci. Rep.* **6**, 32072.
- Morrison, B. H., Haney, R., Lamarre, E., Drazba, J., Prestwich, G. D. and Lindner, D. J. (2009). Gene deletion of inositol hexakisphosphate kinase 2 predisposes to aerodigestive tract carcinoma. *Oncogene* **28**, 2383–2392.
- Parvinen, M. (2005). The chromatoid body in spermatogenesis. *Int. J. Androl.* **28**, 189–201.
- Pouillon, V., Hascakova-Bartova, R., Pajak, B., Adam, E., Bex, F., Dewaste, V., Van Lint, C., Leo, O., Erneux, C. and Schurmans, S. (2003). Inositol 1,3,4,5-tetrakisphosphate is essential for T lymphocyte development. *Nat. Immunol.* **4**, 1136–1143.
- Reuter, M., Berninger, P., Chuma, S., Shah, H., Hosokawa, M., Funaya, C., Antony, C., Sachidanandam, R. and Pillai, R. S. (2011). Miwi catalysis is required for piRNA amplification-independent LINE1 transposon silencing. *Nature* **480**, 264–267.
- Rousseaux, S., Reynoird, N., Escoffier, E., Thevenon, J., Caron, C. and Khochbin, S. (2008). Epigenetic reprogramming of the male genome during gametogenesis and in the zygote. *Reprod. Biomed. Online* **16**, 492–503.
- Russell, L. D., Ettlin, R. A., Hikim, A. P. S. and Clegg, E. D. (1990). *Histological and Histopathological Evaluation of the Testis*. Clearwater, FL: Cache River Press.
- Saiardi, A., Erdjument-Bromage, H., Snowman, A. M., Tempst, P. and Snyder, S. H. (1999). Synthesis of diphosphoinositol pentakisphosphate by a newly identified family of higher inositol polyphosphate kinases. *Curr. Biol.* **9**, 1323–1326.
- Saiardi, A., Nagata, E., Luo, H. R., Snowman, A. M. and Snyder, S. H. (2001). Identification and characterization of a novel inositol hexakisphosphate kinase. *J. Biol. Chem.* **276**, 39179–39185.
- Saunders, P. T. K., Millar, M. R., Maguire, S. M. and Sharpe, R. M. (1992). Stage-specific expression of rat transition protein 2 mRNA and possible localization to the chromatoid body of step 7 spermatids by in situ hybridization using a nonradioactive riboprobe. *Mol. Reprod. Dev.* **33**, 385–391.
- Schmittgen, T. D. and Livak, K. J. (2008). Analyzing real-time PCR data by the comparative C(T) method. *Nat. Protoc.* **3**, 1101–1108.
- Tanaka, T., Hosokawa, M., Vagin, V. V., Reuter, M., Hayashi, E., Mochizuki, A. L., Kitamura, K., Yamanaka, H., Kondoh, G., Okawa, K. et al. (2011). Tudor domain containing 7 (Tdrd7) is essential for dynamic ribonucleoprotein (RNP) remodeling of chromatoid bodies during spermatogenesis. *Proc. Natl. Acad. Sci. USA* **108**, 10579–10584.
- Thomas, M. P. and Potter, B. V. L. (2014). The enzymes of human diphosphoinositol polyphosphate metabolism. *FEBS J.* **281**, 14–33.
- Tseden, K., Topaloglu, O., Meinhardt, A., Dev, A., Adham, I., Müller, C., Wolf, S., Böhm, D., Schlüter, G., Engel, W. et al. (2007). Premature translation of transition protein 2 mRNA causes sperm abnormalities and male infertility. *Mol. Reprod. Dev.* **74**, 273–279.
- Vasileva, A., Tiedau, D., Firooznia, A., Müller-Reichert, T. and Jessberger, R. (2009). Tdrd6 is required for spermiogenesis, chromatoid body architecture, and regulation of miRNA expression. *Curr. Biol.* **19**, 630–639.
- Verbsky, J., Lavine, K. and Majerus, P. W. (2005a). Disruption of the mouse inositol 1,3,4,5,6-pentakisphosphate 2-kinase gene, associated lethality, and tissue distribution of 2-kinase expression. *Proc. Natl. Acad. Sci. USA* **102**, 8448–8453.
- Verbsky, J. W., Chang, S.-C., Wilson, M. P., Mochizuki, Y. and Majerus, P. W. (2005b). The pathway for the production of inositol hexakisphosphate in human cells. *J. Biol. Chem.* **280**, 1911–1920.
- Wang, H., DeRose, E. F., London, R. E. and Shears, S. B. (2014). IP6K structure and the molecular determinants of catalytic specificity in an inositol phosphate kinase family. *Nat. Commun.* **5**, 4178.
- Wilson, M. P., Hugge, C., Bielinska, M., Nicholas, P., Majerus, P. W. and Wilson, D. B. (2009). Neural tube defects in mice with reduced levels of inositol 1,3,4-trisphosphate 5/6-kinase. *Proc. Natl. Acad. Sci. USA* **106**, 9831–9835.
- Xu, Q., Lin, H.-Y., Yeh, S.-D., Yu, I.-C., Wang, R.-S., Chen, Y.-T., Zhang, C., Altuwajiri, S., Chen, L.-M., Chuang, K.-H. et al. (2007). Infertility with defective spermatogenesis and steroidogenesis in male mice lacking androgen receptor in Leydig cells. *Endocrine* **32**, 96–106.

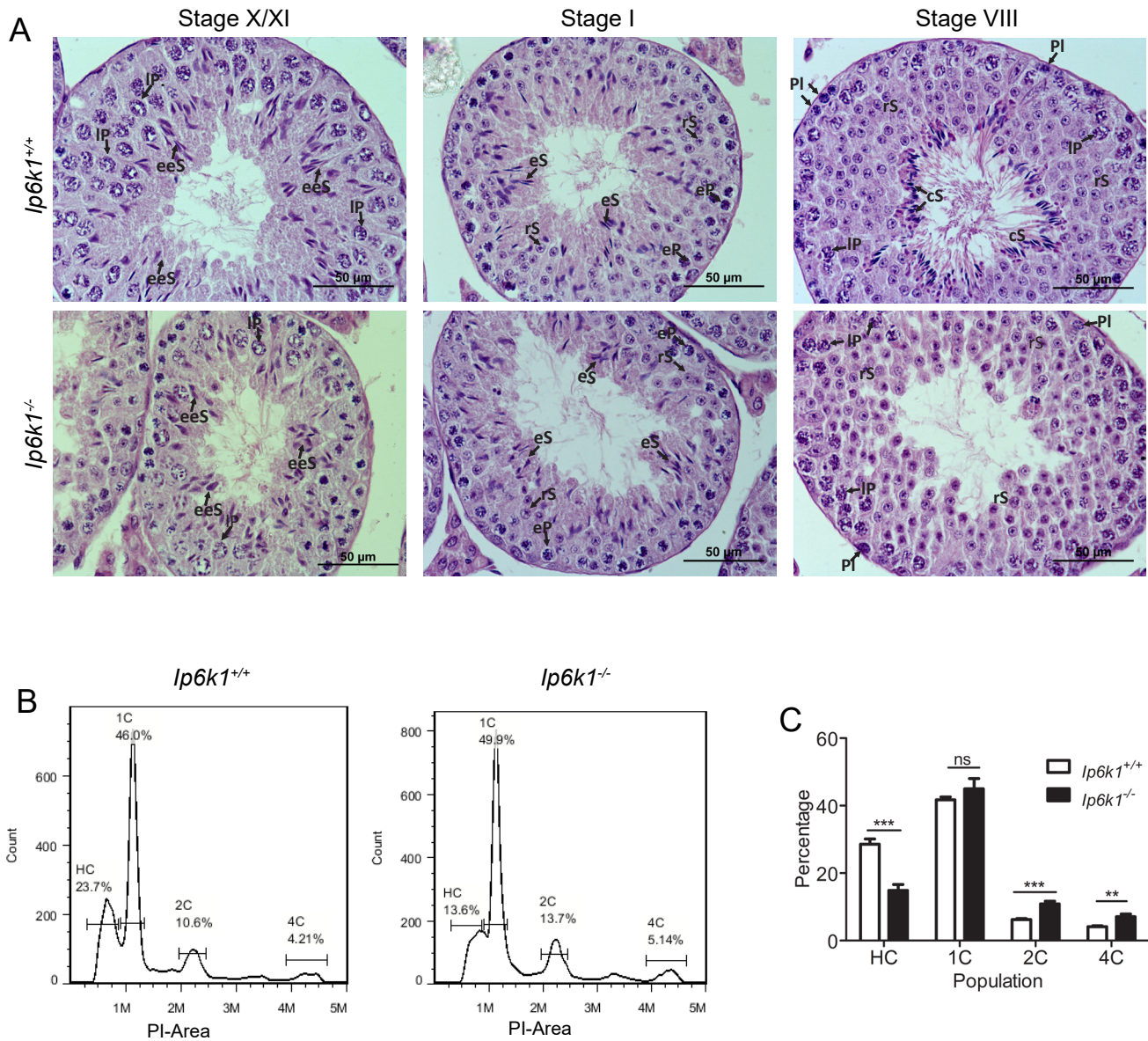


Figure S1. Condensed spermatids are absent in *Ip6k1*^{-/-} testes.

(A) Haematoxylin and eosin stained testes cross sections of 2 month old *Ip6k1*^{+/+} and *Ip6k1*^{-/-} mice. The stage of the seminiferous epithelium was determined for each tubule cross section by examining the presence, morphology and position of different cell types. For *Ip6k1*^{-/-} sections, where the programme of spermiogenesis is disrupted, sections were staged based on cells other than elongating/elongated spermatids. Individual cell types are marked in bold black letters. PI - preleptotene spermatocytes; eP - early pachytene spermatocytes; IP- late pachytene spermatocytes; rS - round spermatids; eeS - early elongating spermatids; eS - elongating spermatids; cS - elongated/condensed spermatids. Scale bar is 50 μ m. (B) Flow cytograms of propidium iodide (PI) stained *Ip6k1*^{+/+} and *Ip6k1*^{-/-} testicular cells showing peaks for elongated spermatids (HC), round spermatids (1C), spermatogonia, secondary spermatocytes and Sertoli cells (2C) and primary spermatocytes (4C). Data are representative of five independent experiments. (C) Relative percentages of HC, 1C, 2C and 4C cell populations in 2 to 4 month old *Ip6k1*^{+/+} and *Ip6k1*^{-/-} mice measured by flow cytometry. Data (mean \pm s.e.m., $n = 5$) were analysed using a two-tailed unpaired Student's t test. *** $P < 0.001$; ** $P < 0.01$; ns, not significant, $P = 0.33$.

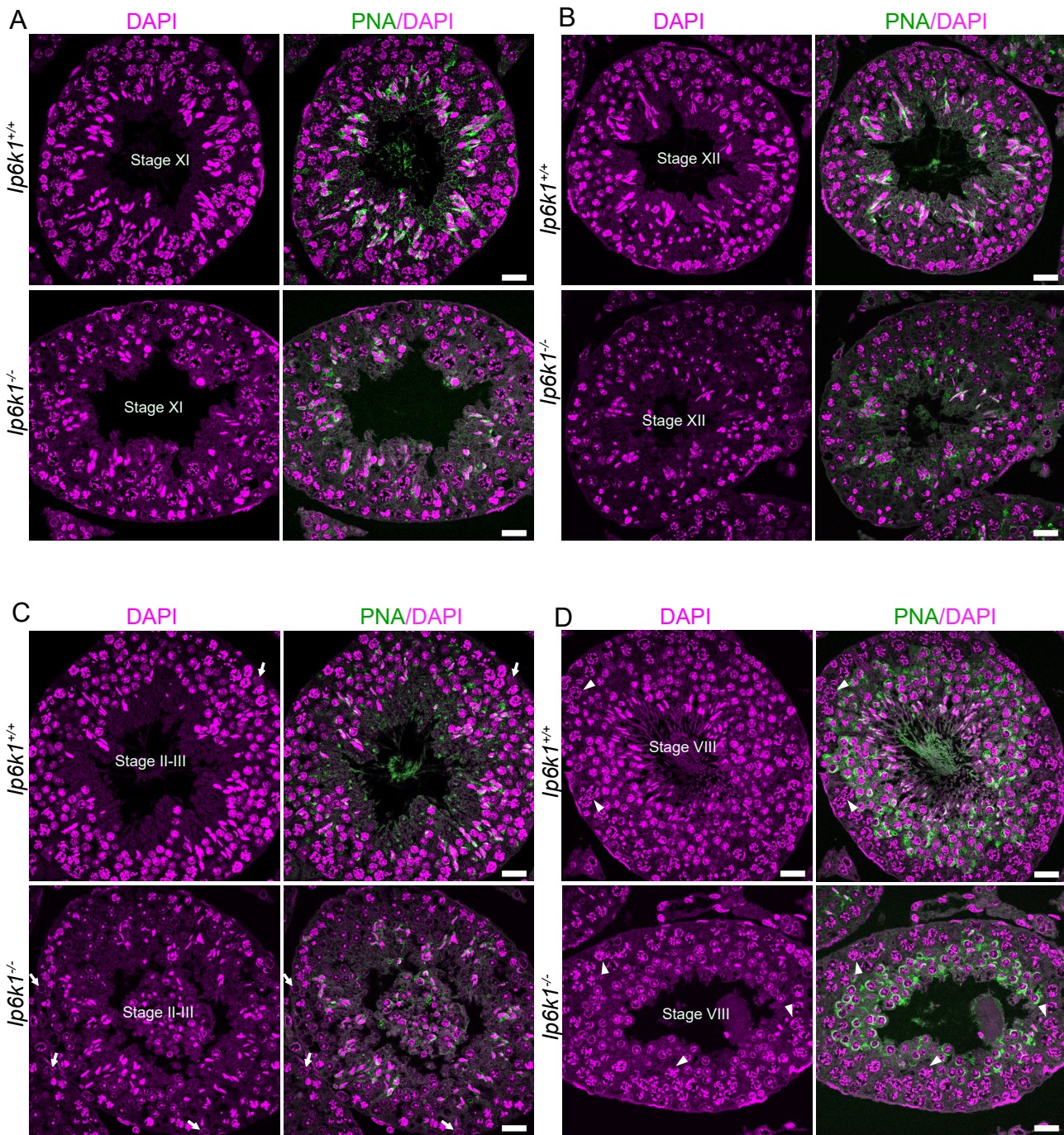


Figure S2. Staging of seminiferous tubules from *Ip6k1*^{+/+} and *Ip6k1*^{-/-} mice.

(A-D) *Ip6k1*^{+/+} and *Ip6k1*^{-/-} testes cross sections were stained with peanut agglutinin (PNA) to detect the outer acrosomal membrane and DAPI to mark nuclei. The white regions indicate the overlap of PNA (green) and DAPI (magenta). The stage of the seminiferous epithelium was determined for each tubule cross section by examining the presence, morphology and position of different cell types. For *Ip6k1*^{-/-} sections, where the programme of spermiogenesis is disrupted, sections were staged based on cells other than elongating/elongated spermatids. Stage XI tubules were identified by the absence of round spermatids and presence of diplotene spermatocytes; stage XII tubules contained secondary spermatocytes; stage II-III tubules were identified based on the pattern of PNA staining in round spermatids and the presence of early pachytene spermatocytes; and stage VIII tubules were identified based on the arc-like staining of PNA in round spermatids. Zoomed in versions of panels (A) to (D) are presented in Figure 3. In panels C and D, arrows indicate spermatogonia and arrowheads indicate primary spermatocytes. Scale bar is 20 μm.

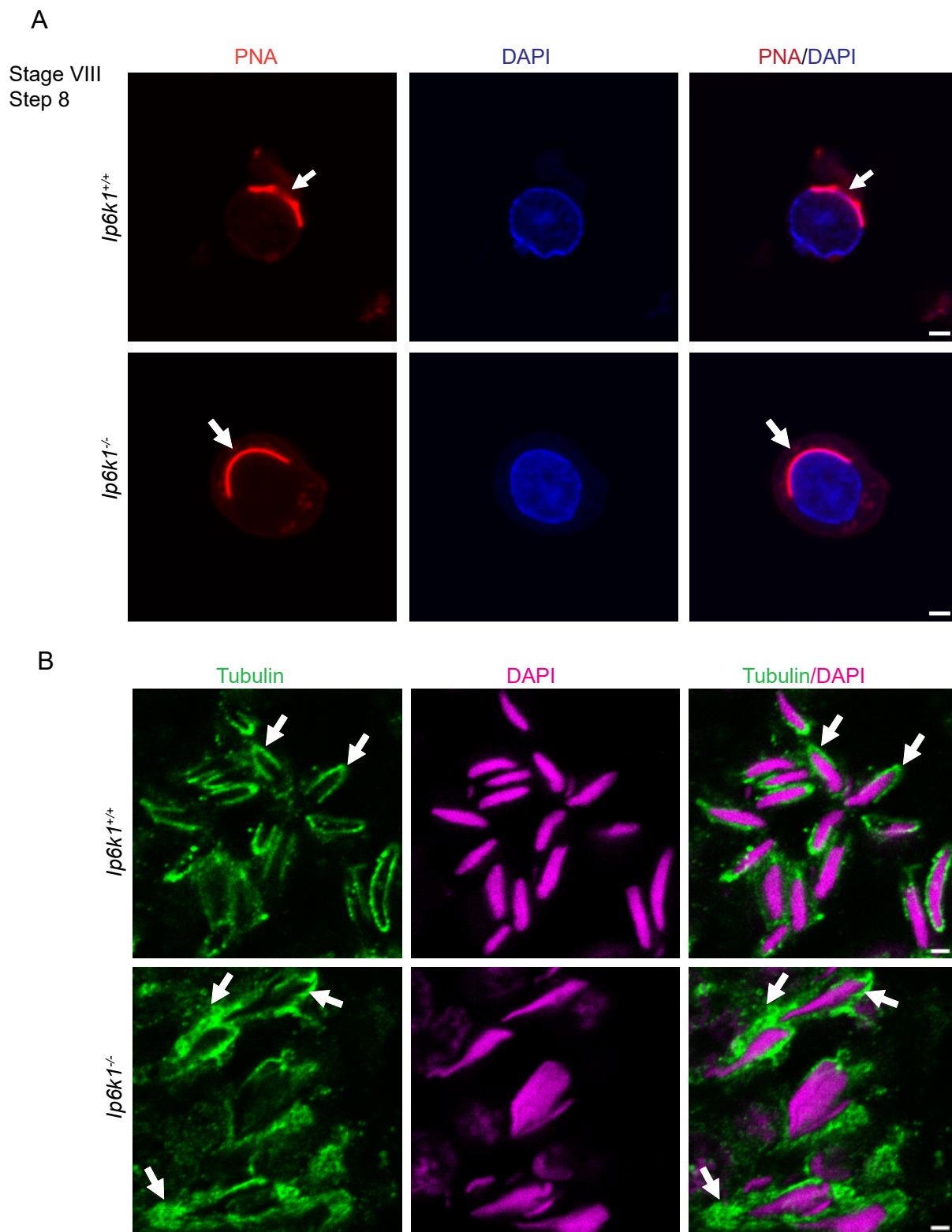


Figure S3. Normal acrosome and manchette development in *Ip6k1^{-/-}* spermatids.

(A) Immunostaining of *Ip6k1^{+/+}* and *Ip6k1^{-/-}* round spermatids with peanut agglutinin (PNA, red). Nuclei were counterstained with DAPI (blue). Round spermatids were isolated from specific stages of seminiferous tubules based on the light absorption pattern (see Methods section) and stained with PNA to detect the acrosome. Arrows show fully formed acrosomes in *Ip6k1^{+/+}* and *Ip6k1^{-/-}* round spermatids. Scale bar is 2 μ m. (B) Testes cross sections of *Ip6k1^{+/+}* and *Ip6k1^{-/-}* mice were immunostained with α -tubulin (green) and the images were focused on elongating spermatids (steps 9 and 10). Arrows indicate the transiently synthesised manchette in *Ip6k1^{+/+}* and *Ip6k1^{-/-}* elongating spermatids. Although the nuclei were abnormally condensed, manchettes were observed in *Ip6k1^{-/-}* elongating spermatids. Nuclei were counterstained with DAPI (magenta). Scale bar is 2 μ m.

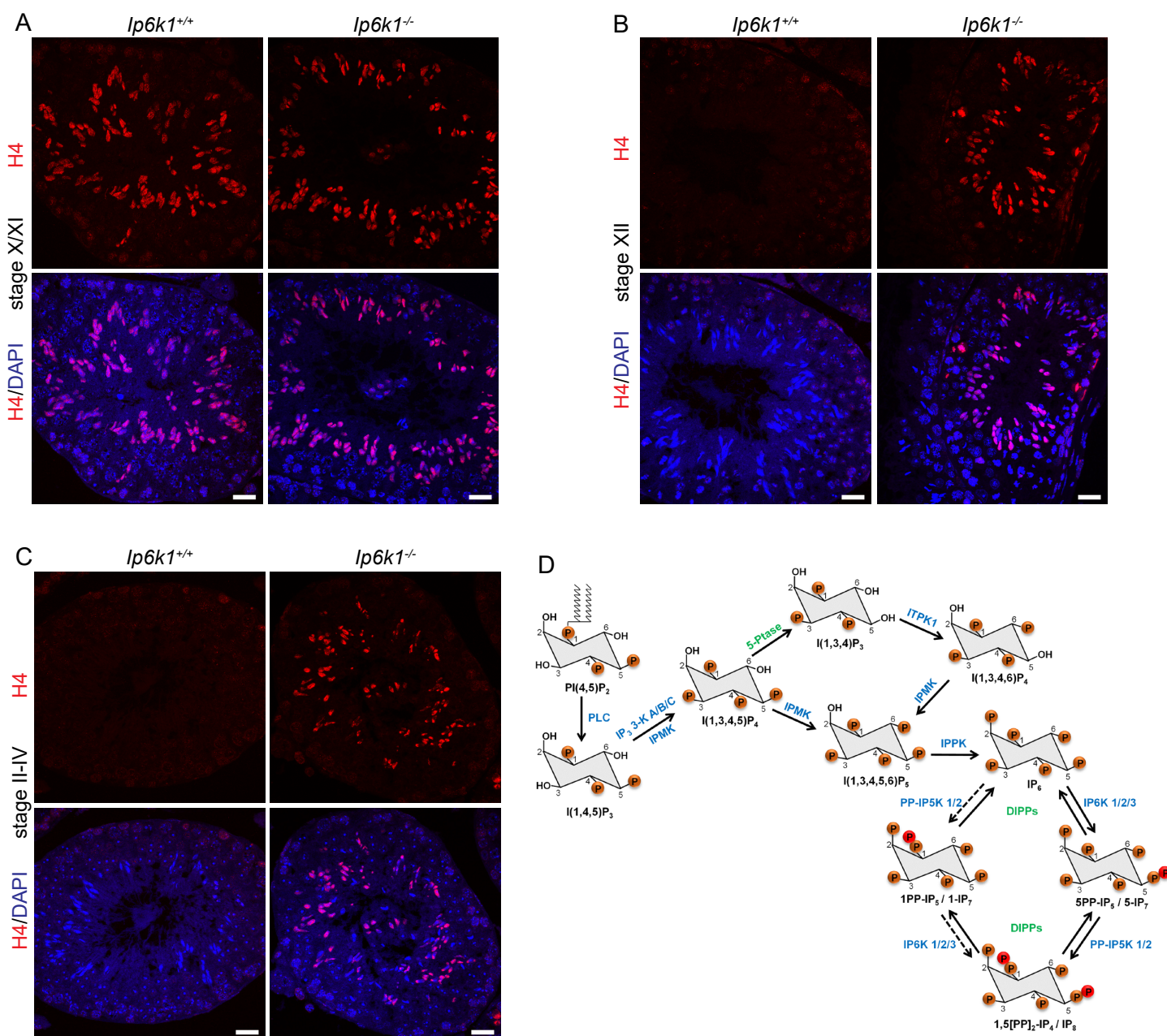


Figure S4 (A-C) Retention of histone H4 in *Ip6k1*^{-/-} elongating spermatids. *Ip6k1*^{+/+} and *Ip6k1*^{-/-} testes cross sections were stained to detect histone H4 (red) and nuclei were stained with DAPI (blue). The stage of the seminiferous epithelium was determined for each tubule cross section by examining the presence, morphology and position of different cell types. For *Ip6k1*^{-/-} sections, where the programme of spermiogenesis is disrupted, sections were staged based on cells other than elongating/elongated spermatids. Stage X/XI tubules were identified by the absence of round spermatids and presence of late pachytene or diplotene spermatocyte; stage XII tubules contained secondary spermatocytes; and stage II-IV tubules were identified based on the presence of round spermatids and early pachytene spermatocytes. Zoomed in versions of panels (A) to (C) are presented in Figure 4. Scale bar is 20 μ m. **(D) Pathway of inositol phosphate biosynthesis in mammals.** I(1,4,5)P₃ generated from PI(4,5)P₂ is the starting point for the synthesis of higher inositol phosphates. The enzymes involved in inositol phosphate synthesis are depicted in blue and dephosphorylating enzymes are depicted in green. The phosphate donor is ATP. Dotted arrows represent minor pathways of inositol phosphate synthesis. Carbon atoms on the myo-inositol ring are numbered from 1 to 6. PLC, phospholipase C; IP₃ 3-K, IP₃ 3-kinase; IPMK, inositol polyphosphate multikinase; 5-Ptase, I(1,3,4,5)P₄ 5-phosphatase; ITPK1, inositol 1,3,4-trisphosphate 5/6 kinase; IPPK, IP₅ 2-kinase; IP6K, inositol hexakisphosphate kinase; PP-IP5K, 5-PP-IP5 kinase; DIPPs, diphosphoinositol polyphosphate phosphohydrolases.